BATTERIES FOR ADVANCED TRANSPORTATION TECHNOLOGIES (BATT) PROGRAM ANNUAL REVIEW JULY 1-2, 2002

PRESENTATION SUMMARIES

Cell Development

K. Striebel (LBNL)	Development of the $LiFePO_4$/Gel/Natural Graphite Cell
T. Richardson (LBNL)	Cell Development Support, Overcharge Protection, Cathode Materials
K. Zaghib (IREQ)	Li-ion Polymer Batteries with Low-Cost Materials

Anodes and Cathodes

M. Thackeray (ANL)	Non-Carbonaceous Anodes
M. Thackeray (ANL)	Novel Cathodes
M.S. Whittingham (SUNY Binghamton)	Novel Anode Materials
M.S. Whittingham (SUNY Binghamton)	Novel Cathode Materials
G. A. Nazri (U. Michigan)	Novel Composite Anodes for Lithium-ion Batteries
M. Doeff (LBNL)	Synthesis and Characterization of Cathode Materials
T. Devine (LBNL)	Aluminum corrosion in Nonaqueous Electrolytes
C. Grey (SUNY Stony Brook)	NMR and First-Principles Calculations of Two-Electron Redox Processes: The Layered Lithium Nickel Manganese Oxides

Electrolytes

N. Balsara, J. Kerr (LBNL)	Polymer Electrolyte Design
S. Khan (NCSU)	Composite Polymer Electrolytes
D. DesMarteau, S. Creager (Clemson Univ.)	New Battery Electrolytes Based on Oligomeric Lithium Bis((perfluoroalkyl)sulfonyl)imide Salts
G. Smith (U. of Utah)	Molecular Dynamics Simulation Study of the Influence of Polymer Structure on Lithium Cation Mobility in Polymer Electrolytes
J. Kerr (LBNL)	Electrolyte Additives

Advanced Diagnostics

R. Kostecki, F. McLarnon (LBNL)	Electrode Surface Layers
J. McBreen (BNL)	Battery Materials: Structure and Characterization
P. Ross (LBNL)	Interfacial and Reactivity Studies
E. Cairns (LBNL)	Cathode Material Studies Using ^7Li NMR

Modeling

J. Newman (LBNL)	Improved Electrochemical Models
A.M. Sastry (U. Michigan)	Modeling of Electrode Failure Modes

Development of the $LiFePO_4$/Gel/Natural Graphite Cell (K. Striebel, LBNL)

The primary objective of the cell fabrication and testing task within the BATT Program is to benchmark the performance of new materials for baseline low-cost gel and Li-ion cell technologies. Novel materials developed within the rest of the BATT Program and elsewhere are tested in a standard cell with preset protocols. Cell components are analyzed with BATT Program diagnostics to provide the necessary link between the invention of novel battery components and the diagnostic evaluation of failure modes, to accelerate the development of a battery-powered electric vehicle.

The LBNL pouch cell design consists of 12-cm^2 single-side coated electrodes with a Celgard separator and liquid or cross-linked gel electrolyte. In addition, 100-mAh cells with the Advanced Technology Development (ATD) Program Gen 2 cell chemistry were received from Quallion, Inc., and 3.8 cm^2 pouch cells with the low-cost baseline chemistry and gel electrolyte were received from Hydro Quebec (IREQ).

Studies with the Li-ion baseline cell (Gen 2) focused on the dependence of capacity fade and area-specific impedance (ASI) upon cycling regimen and temperature. Capacity fade rates for pouch cells with EC-DMC-$LiPF_6$ (LP40) electrolyte are similar to those for the 100-mAh Quallion cells, and thereby verify our pouch cell design. The PNGV Power-Assist Life-Cycle Profile leads to negligible power fade, and lower rates of capacity fade (as compared to 100%-DOD cycling) for these cells. In addition, a cell cycled at 80% DOD for 1000 cycles showed no capacity loss (*i.e.*, >80% capacity remained). A pouch cell cycled at 60°C (cell ID no. PG13) has been analyzed in detail. The cathode showed capacity loss even when removed from the cell and cycled against fresh Li, probably due to a loss of conductivity and/or film formation on the cathode.

The bulk of work in FY 2002 focused on the evaluation of the performance and cycle life of $LiFePO_4$ cells with natural graphite anodes and either liquid (LBNL) or gel (IREQ) electrolyte, see Fig. 1. The cells assembled with $LiPF_6$/carbonate electrolyte showed higher capacity due to a moderate irreversible capacity loss (ICL) and higher electrolyte conductivity. The $LiBF_4$-containing cells either with gel or liquid solvents showed large ICL. All cells showed an unacceptable rate of capacity fade. For the gel cells, calendar-life studies showed that both the capacity fade and impedance rise were functions of time, and did not arise from cycling-induced stress. Electrochemical diagnostics of the electrodes revealed that a side reaction is consuming the cycleable Li in the system while the electrode structure remains intact. The LBNL-made $LiFePO_4$ electrodes showed good formation behavior but poorer high-rate utilization than the IREQ-made electrodes. The ASI values measured for the gel cells were lower than those for the liquid-electrolyte cells, suggesting that the interfaces formed with the gel electrolyte exhibit lower impedance.

Future work will focus on understanding the behavior of the natural graphite anode in the baseline electrolytes, the addition of additives, the preparation of good high-rate utilization electrodes from low-conductivity materials, and the evaluation of $LiFePO_4$ with different particle morphologies from IREQ and other sources, as well as anode and cathode materials received from BATT Program researchers.

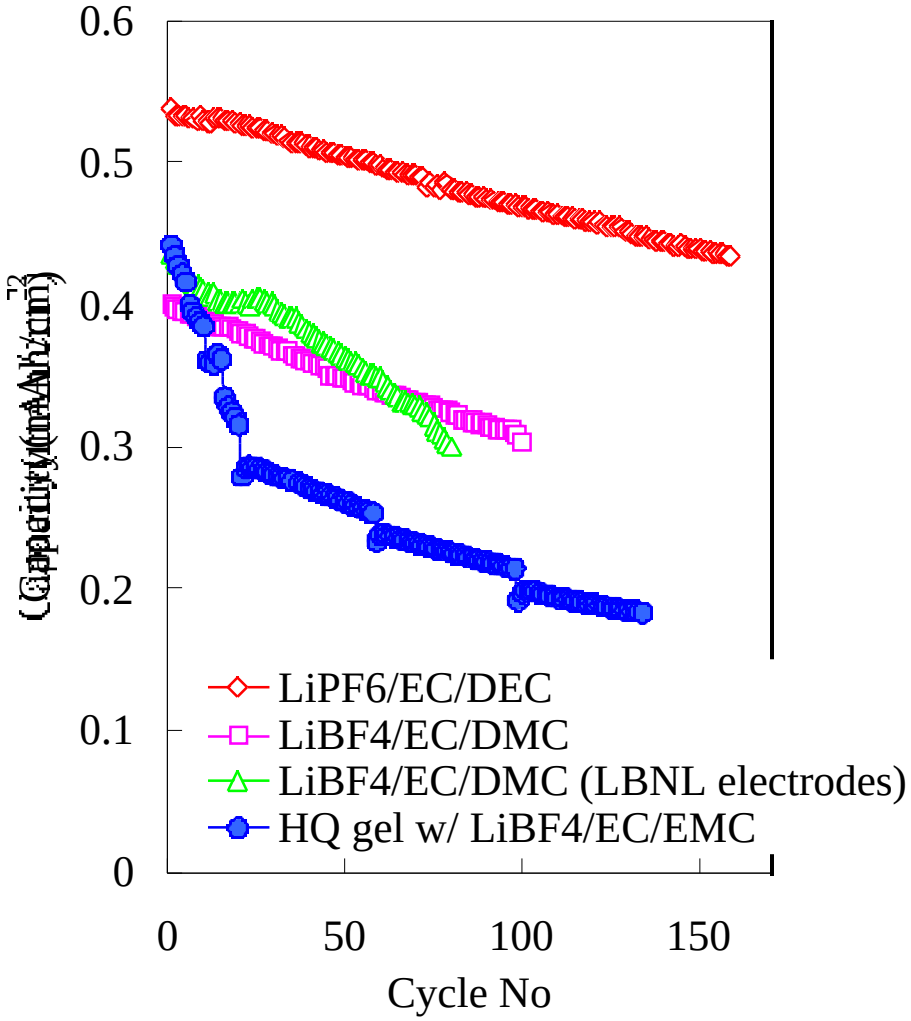

Figure 1. Low-cost baseline cell with $LiFePO_4$/natural graphite. Plotted are the capacity and fade rate *vs.* electrolyte composition, for constant-current C/2 cycling at 100% DOD and 25°C between 2.5 and 4.0V, for low-cost baseline cells with four different electrolytes. All electrodes were prepared by IREQ unless noted otherwise. $LiPF_6$ electrolytes show higher capacity due to higher conductivity and lower ICL. The gel electrolyte cell shows evidence of a chemical side reaction consuming the cycleable Li in the system.

Cell Development Support, Overcharge Protection, Cathode Materials (T. Richardson, LBNL)

This work is divided into three subtasks:

Support cell development through structural characterization of active electrode components

Feedstock powders and electrodes from cycled cells were examined by X-ray diffraction (XRD) and infrared spectroscopy (IR). XRD provided information on electrode state of charge, homogeneity, degradation of crystallinity, deleterious phase transitions, as well as the accumulation of electrode, current collector, or electrolyte decomposition products. IR spectra are also sensitive to state of charge, and can reveal the presence of poorly crystalline or amorphous components not detected by XRD. Because the sample size is small, IR can also detect spatial inhomogeneity across the electrode.

Develop an inexpensive, self-actuating overcharge protection mechanism

Although the redox shuttle additives studied in our previous work can provide limited overcharge protection for storage batteries charged at low rate (C/3), a high-current internal protection mechanism is needed for multicell stacks. Certain electroactive polymers can switch between resistive and nearly metallic states through reversible electrochemical redox reactions. A 50-μm-thick poly-3-methylthiophene shunt produced by electropolymerization within a porous polypropylene separator was able to carry a current of 5 mA/cm^2 between a stainless steel positive and Li negative electrode at a cell potential of less than 5 V.

Synthesize and evaluate alternative electrode materials

Manganese and iron phosphates with the alluaudite structure (Fig. 2) were prepared by solid-state reactions. $Na_2Mn_2Fe(PO_4)_3$, $LiNaMn_2Fe(PO_4)_3$, and $NaFe_3(PO_4)_3$ are previously unreported phases. $Li_2Mn_2Fe(PO_4)_3$ was prepared from $Na_2Mn_2Fe(PO_4)_3$ by ion exchange. $Na_2Mn_3(PO_4)_3$ (also new) has the related fillowite structure. These materials have a 1:1 metal:phosphate ratio like $LiFe(Mn)PO_4$, but have more-complex structures that can accommodate mixed transition metal oxidation states. They are of interest because of their somewhat higher electronic conductivity, high intercalant ion mobility, and ease of preparation (in air, short heating times). Initial electrochemical tests have been disappointing. Milling to reduce particle sizes and surface coatings may give better results.

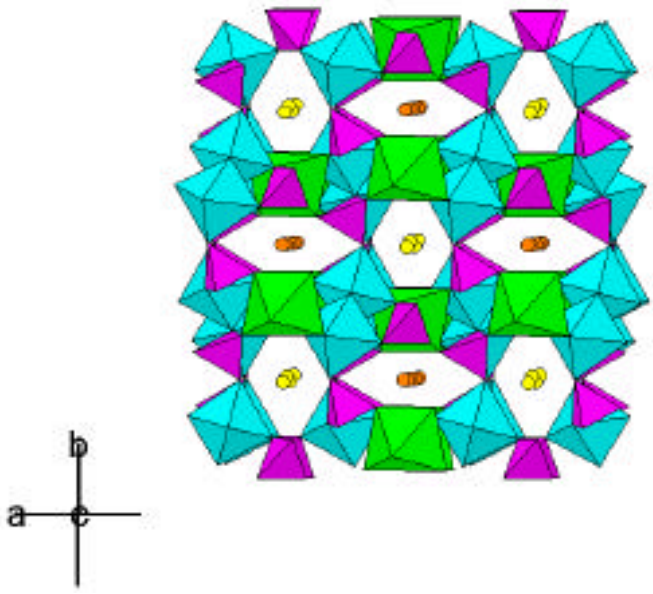

Alluaudites: $Li_xNa_{1-x}Mn_yFe_{3-y}(PO_4)_3$

- ✓ Inexpensive: prepared in air by melt-quenching (fast and easy)
- ✓ Same metal-phosphate ratio as $LiFePO_4$
- ✓ Theoretical capacity 170 mAh/g
- ✓ High ion mobility, probable higher electronic conductivity than $LiFePO_4$
- ✓ Can accommodate mixed oxidation states

Figure 2. New phosphate-stabilized cathodes

Li-ion Polymer Batteries with Low-Cost Materials (K. Zaghib, Hydro-Québec Research Institute, IREQ)

We have completed the physicochemical and electrochemical characterization of low-cost $LiFePO_4$ synthesised at the University of Montreal (UM). The composition of positive and negative electrodes were optimized (*i.e.*, proportion of binders, conductive agent, and active materials), and the electrode materials coated on Al and Cu current collectors, respectively, to obtain the desired capacity balance with 10-20% excess anode material. The UM $LiFePO_4$ cathode material, surface treated with <2 wt% carbon, was evaluated at 25°C with gel electrolyte. This cathode delivered a reversible capacity of 160 mAh/g (10 mAh/g lower than the theoretical capacity) at the C/24 rate.

Several gel-type Li-ion cells were prepared, and 30 cells were sent to LBNL for evaluation (Fig. 3). In addition, positive and negative electrodes containing $LiFePO_4$ and natural graphite, respectively, were sent to LBNL. The effect of cell compression on the electrode performance was studied in two different cell configurations: Li/gel polymer/graphite, and Li/gel polymer/$LiFePO_4$ without Celgard membranes. The effect of pressure on the first-cycle ICL is shown in Fig. 4. Not shown is the drop-off in reversible capacity for the anode and cathode at 20 and 30 psi, respectively. From these studies, and impedance measurements, an optimum compression of 10 psi was determined and used for the remainder of cell testing.

Figure 3. IREQ gel-type Li-ion cell

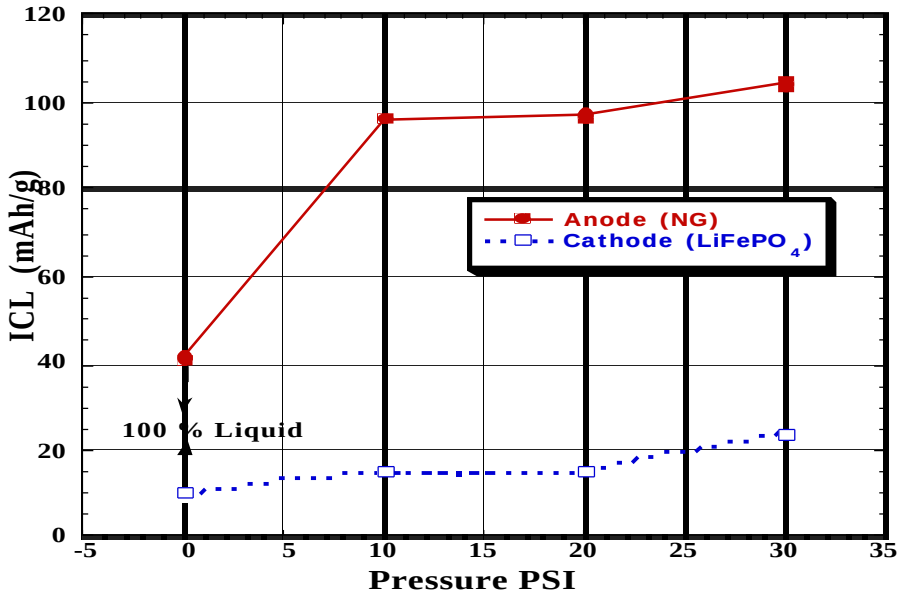

Figure 4. Dependence of first-cycle ICL on cell compression with gel electrolyte and a Li anode

Non-Carbonaceous Anodes (M. Thackeray, ANL)

The objective of this task is to find an alternative, low-cost intermetallic anode to replace carbon and to improve the overall safety of Li-ion cells. The approach has been to search for intermetallic systems that operate a few hundred mV above the potential of metallic Li (and lithiated graphite) without compromising the capacity of the anode or the energy of the cell. Because of their relatively high densities, intermetallic electrodes offer significantly superior volumetric capacities to carbon. The goals of the project during FY 2002 were to achieve a specific capacity of 300 mAh/g and a volumetric capacity of 2000 mAh/ml for 100 cycles in a Li/intermetallic cell at 0.5-1.0 V above the potential of metallic Li.

Over the past two years, the strategy that has been adopted to improve electrochemical performance has been to search for intermetallic systems in which strong structural relationships exist between the parent and the lithiated electrodes; the reactions that occur in these systems can therefore be regarded as topotactic. Such an approach is consistent with the need to keep the structural changes of transition metal oxide positive electrodes, such as the layered $LiMO_2$ (M=Co, Ni, Mn) and spinel $LiMn_2O_4$-type compounds, to an absolute minimum during Li insertion and extraction.

During FY 2002, the search for new or modified systems with improved electrochemical and structural properties was continued. Efforts were focused predominantly on two systems, 1) substituted $Cu_6M_xSn_5$ (M=Fe, Ni, Zn) electrodes and 2) MnSb. In addition, efforts were made to understand the root causes for the ICL effects that are observed in all intermetallic systems. For the capacity-loss studies, Cu_2Sb electrodes were used. Oxide passivation coatings were found contribute minimally to capacity-loss effects, as did attempts to vary the porosity of the electrodes. Several electrolytes were investigated; EC/DEC and EC/EMC provided the best performance. Other studies that are in progress and will continue in FY 2003 include 1) investigating the effect of adding excess metal to the electrode to compensate for some of the metal that is irreversibly extruded from the host array of the intermetallic electrode during the initial reaction, 2) understanding the effect of binders and the electronic isolation of electrode particles, and 3) studying the effect of adding electronically conducting additives in an attempt to counter the electronic isolation of the electrode particles.

MnSb electrodes were investigated electrochemically and by *in situ* X-ray diffraction (XRD). These electrodes show a lower ICL on the initial cycle (15-20%) compared to many other intermetallic electrodes such as Cu_6Sn_5, Cu_2Sb, and InSb (25-40%). A stable rechargeable capacity, slightly in excess of 300 mAh/g has been achieved; the targeted cycle life has not yet been demonstrated. *In situ* XRD data showed that MnSb electrodes react topotactically with Li in essentially two stages. Lithium insertion into the NiAs-type structure of MnSb first induces a transformation to LiMnSb with an ordered anti-fluorite-type structure; thereafter, Li is inserted into, and Mn extruded from, a face-centered-cubic Sb array to yield Li_3Sb. The proposed structural transformations associated with these two reactions, which are reversible, are shown schematically in Fig. 5.

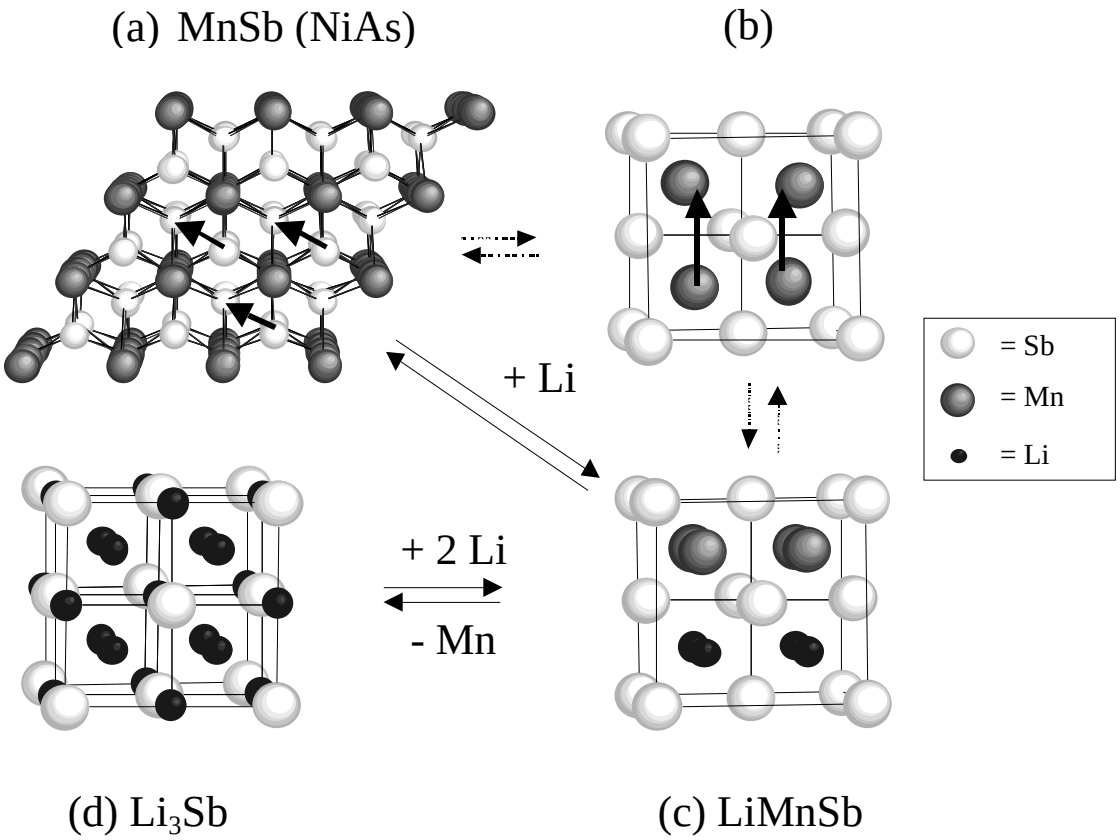

Figure 5. The proposed reaction sequence for the transformation of (a) MnSb (NiAs-type structure) to (d) Li_3Sb via (c) an intermediate LiMnSb (ordered anti-fluorite) structure. The transformation of the MnSb framework in the parent NiAs-type structure to the MnSb framework in LiMnSb can occur *via* a zinc-blende MnSb framework that requires the displacement of 50% of the Sb atoms, which is similar to the process in the Cu_6Sn_5-to-Li_2CuSn transition.

Novel Cathode Materials (M. Thackeray, ANL)

The objective of this task is to develop a low-cost manganese oxide to replace $LiCoO_2$ as the cathode material of choice for Li-ion cells. Our approach has been to exploit the concept of using a Li_2MnO_3 component to stabilize layered $LiMO_2$ electrode structures (M=Mn, Ni, Co) with the ultimate goal of stabilizing a layered $LiMnO_2$ electrode. This approach has led to the search for stable composite electrode structures that, in general, can be formulated as having the composition $xLi_2MnO_3 \cdot (1-x)LiMO_2$. During the year, it became widely known that similar, but not identical, approaches were also being conducted by leading Li-ion battery research groups around the world. The specific goal set for FY 2002 was to achieve a specific capacity of 160 mAh/g for 100 cycles at 50°C. At the time of the BATT Program review, some electrodes had attained the targeted capacity for 65 cycles in cells that were still in operation; it was anticipated that the capacity goal would be achieved by September 2002.

The strategy to stabilize layered $LiMO_2$ electrode structures was broadened during FY 2002 to include stabilizing components that were isostructural with Li_2MnO_3, in particular, Li_2TiO_3 and Li_2ZrO_3. These three compounds are generally regarded as being essentially electrochemically inactive at the typical operating voltage of Li-ion cells (3.0 to 4.2 V). In addition, preliminary studies of isostructural Li_2RuO_3 electrodes, which are electrochemically active at 4 V *vs*. Li, were undertaken. However, the major focus of the effort in FY 2002 was placed on the characterization of $xLi_2M'O_3 \cdot (1-x)LiMO_2$ electrodes in which M′ was either Ti or Zr, and the $LiMO_2$ component was $LiMn_{0.5}Ni_{0.5}O_2$. These "composite" electrode systems have provided rechargeable capacities of approximately 140-150 mAh/g at room temperature and significantly higher capacities (160-180 mAh/g) at 50°C. During the course of these studies, it was discovered that the parent compound, $LiMn_{0.5}Ni_{0.5}O_2$, as well as the composite electrodes $xLi_2TiO_3 \cdot (1-x)LiMn_{0.5}Ni_{0.5}O_2$ could accommodate additional Li at approximately 1.5 V *vs*. Li to yield a hexagonal-close-packed Li_2MO_2-type structure in which the lithium occupies tetrahedral sites between sheets of MO_6 octahedra. A schematic phase diagram showing the change in composition of the $xLi_2M'O_3 \cdot (1-x)LiMO_2$ composite electrode during charge and discharge is shown in Fig. 6; during lithium insertion and extraction, the layered arrangement of the transition metal ions remains unaltered thereby providing a remarkably stable electrode over a very wide compositional range. When charged and discharged between 4.6 and 1.45 V, a capacity in excess of 275 mAh/g was achieved. This finding has implications for using the excess lithium in Li_2MO_2-type electrode structures to combat the ICL that is observed on the initial cycle at both carbon and intermetallic electrodes. *In situ* X-ray absorption data collected at the ANL Advanced Photon Source showed that $Li_xMn_{0.5}Ni_{0.5}O_2$ electrodes operate predominantly off two-electron couples, Ni^{4+}/Ni^{2+} between 4.6 and 2.5 V ($0<x<1$), and Mn^{4+}/Mn^{2+} between 2.5 and 1.0 V ($1<x<2$). The high capacities delivered by composite $xLi_2TiO_3 \cdot (1-x)LiMn_{0.5}Ni_{0.5}O_2$ electrodes, particularly for $x=0.31$, strongly suggest that some of the capacity at ~1.5 V is derived from a Ti^{4+}/Ti^{3+} couple.

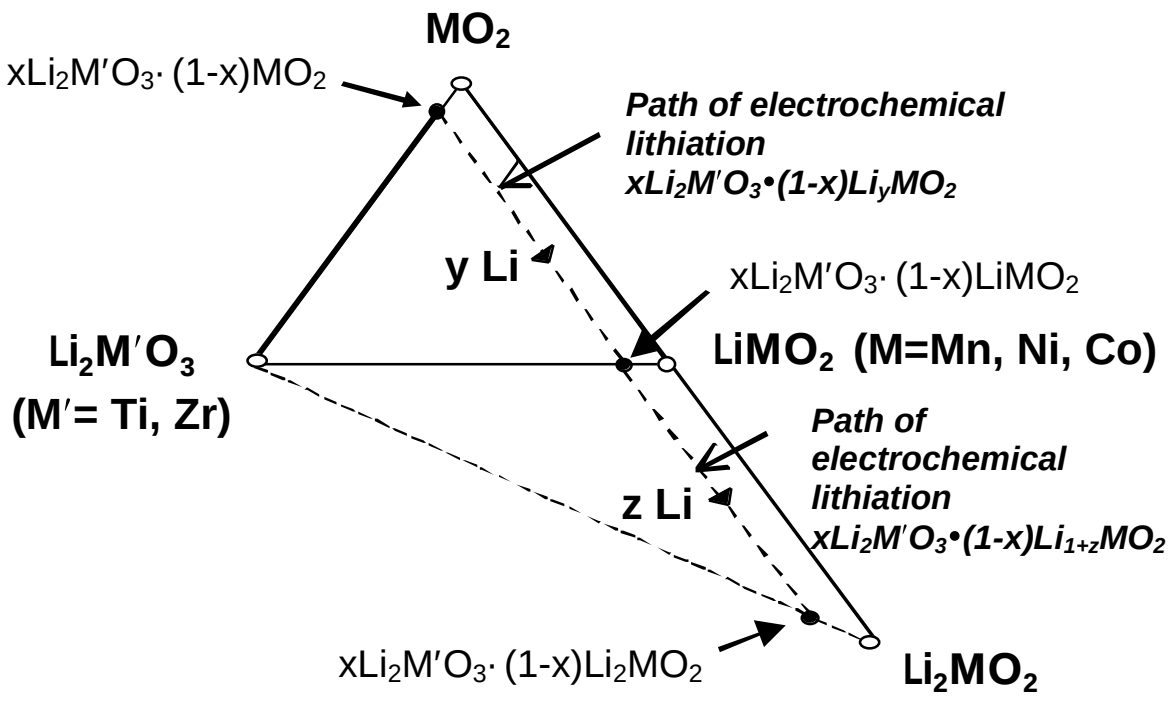

Figure 6. A schematic phase diagram showing the changes in composition of $xLi_2M'O_3 \cdot (1-x)Li_2MO_2$ electrodes during charge and discharge.

Novel Anode Materials (M. S. Whittingham, SUNY at Binghamton)

Our objective is to replace the presently used carbon anodes with safer materials that will be compatible with manganese oxide cathodes and the associated electrolyte. Our approach is to better understand the cause for capacity fade in simple metal alloy/composite anode systems, to remediate capacity fade during cycling, and then to identify a new material that has a higher volumetric capacity than carbon at about 0.5 V *vs*. pure Li.

Our strategy is to study a range of tin compounds in carbonate-based electrolytes. The cells will initially be kept simple by using wherever possible foils of the materials rather than powders, where the binder and/or conductive diluent may play key roles. Pure tin foil is being used as the reference standard; surprisingly little is known about its anode electrochemistry. It's behavior will be compared with a full range of other "materials":

- Sn_2Mn – a single-phase material where the Mn does not react with Li.
- SnBi – a eutectic where particle size can be controlled and both elements react with Li.
- SnSb – a binary compound, where both elements react with Li.
- Cu_6Sn_5 – an electrochemically active insertion compound, studied by Thackeray *et al*.

Data are being collected on the first two, and literature data will be used for the latter two. We also monitor work on tin compounds that are being investigated for use as lead-free solders in the electronics industry.

Pure tin foil: Although tin has been studied in powder form, little is known about its bulk behavior. Figure 7 shows the capacity of pure tin foil at 0.8 and 3.0 mA/cm^2 for the first 10 cycles. The first Li insertion shows only a single discharge plateau, the expected phases at low Li contents are seen in the subsequent cycles but the maximum Li content is only about 3.6 Li/Sn and not the expected $Li_{4.4}Sn$.This high rate capability is not unexpected considering the 10^{-7} cm^2/sec diffusion coefficient. This cycling capacity is much better than past reports; however, the capacity falls off dramatically after about 15 cycles.

Sn_2Mn: Sn_2Mn was formed in a variety of ways, including arc-melting followed by rolling into a thin film metallic electrode. The initial capacity exceeds 500 Ah/kg, and again shows a single discharge plateau upon initial reaction, and just like tin the maximum capacity is about 3.5 Li/Sn. The capacity is maintained for ~10 cycles, as reported by Dahn, *et al* for powdered samples. Upon Li removal the compound Sn_2Mn is reformed.

SnBi eutectic: A rolled metallic sheet of "SnBi" was examined, and it was found that the XRD pattern of the sheet anode before Li insertion and after the first cycle are essentially the same, indicating no change in particle size. The XRD pattern showed the initial formation of Li_3Bi, followed by formation of LiSn, other intermediate phases, and finally "$Li_{3.6}Sn$".

Conclusions: This initial data indicate that tin, unlike aluminum, can cycle for more than 10 cycles at full capacity in carbonate electrolytes. As indicated in Fig. 7, tin foil appears to cycle better than electrodeposited tin (Tamura, *et al*), is better than our initial data for Sn_2Mn, and the capacity is equivalent to tin annealed at 200°C (i.e. Cu_6Sn_5). The change of impedance upon cycling is being studied, and electrolyte changes are being monitored.

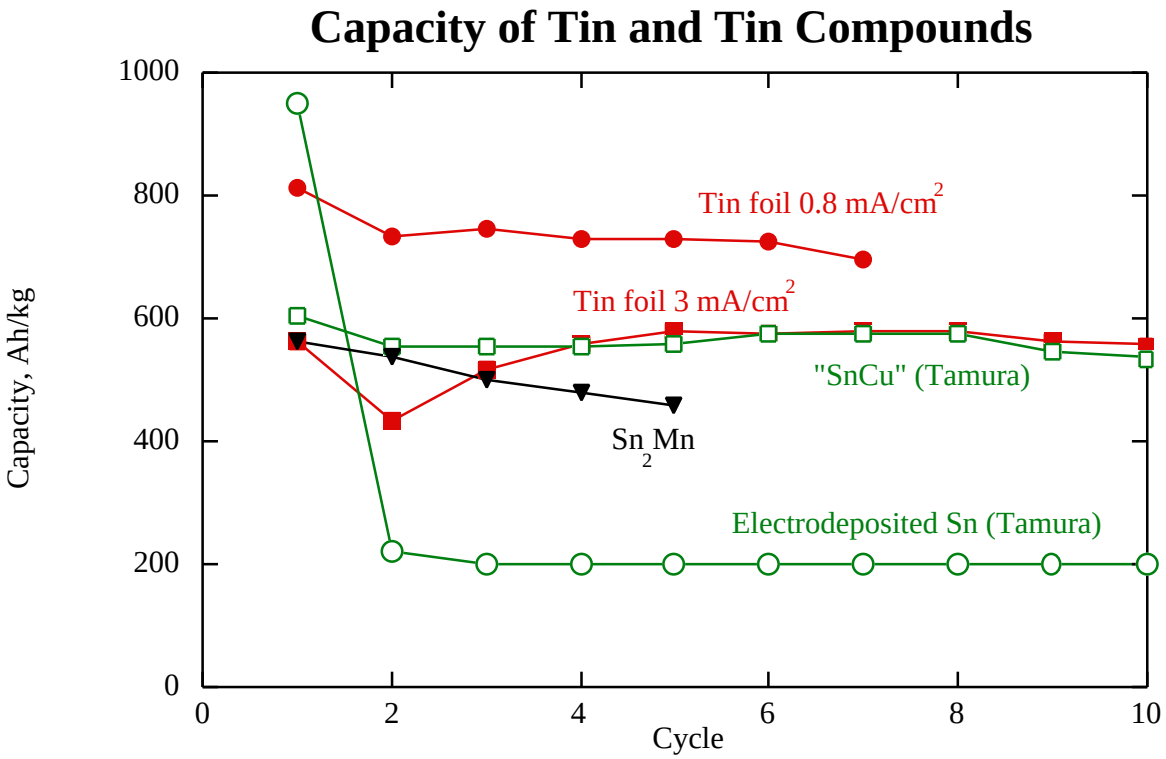

Figure 7. Comparison of capacity of Sn foil at 0.8 and 3.0 mA/cm^2 with Sn_2Mn and electrodeposited Sn and Sn annealed on Cu ("SnCu") [from Tamura et al, *J. Power Sources*, **107**, 48 (2002)]. Note that Tamaru's data were corrected for the weight of Cu assuming a 1:1 Sn:Cu ratio.

Novel Cathodes (M. S. Whittingham, SUNY at Binghamton)

Our emphasis remains on low-cost materials with capacities approaching 200 mAh/g, in particular layered manganese oxides. In addition, $LiFePO_4$ was studied as a low-cost intermediate-capacity system and δ-vanadium oxides as a very high capacity system.

Iron Phosphate – low-cost baseline 150 mAh/g cathodes.

We emphasized $LiFePO_4$ as a comparison standard for our efforts to develop new cathodes. Hydrothermal synthesis was not found to be a viable preparative procedure due to lattice iron disorder. We evaluated $LiFePO_4$ electrochemical stability upon overdischarge and found that Li_3PO_4 is formed which is not reversible. 100 % capacity is readily attained at 0.1 mA/cm^2, dropping to 80% at 1 mA/cm^2 with loadings of 20 to 80 mg/cm^2. The method of carbon coating was not found to be important, and carbon levels of 6 to 12 wt % were found to be effective. Using carbon coatings, the capacity was increased to 100% at 1 mA/cm^2 at 50°C. The capacity/rate relationship is shown in Fig. 8. Capacity retention during cycling is very good. Samples have been provided to LBNL for evaluation. A wide range of other iron phosphates has been studied, including amorphous iron phosphate and giniite, where other transition metals can be substituted for the iron. However, $LiFe_{1-y}Mn_yPO_4$ was not particularly attractive, cycling ≈ 0.5 Li at steady state.

Stabilized manganese oxide cathodes – low cost, high capacity, safe systems

We are exploring both the geometric and electronic approaches to the stabilization of layered manganese dioxide. In the former we found that vanadium oxide pillars prevented the formation of spinel-like phases. The rate capability requires enhancing, and we are using cobalt to achieve this. In the electronic approach, we make $LiMnO_2$ behave more like $LiCoO_2$ by substituting an element to the right of Co in the Periodic Table, such as Ni. Earlier we showed that such doping by nickel, iron, or cobalt enhances the electronic conductivity and cyclability of the manganese oxide. However, 10% substitution did not prevent spinel formation. Higher levels, ≥ 50%, as in $LiMn_{0.4}Ni_{0.4}Co_{0.2}O_2$, were found to maintain the layered structure. This compound cycled well with capacities approaching 200 Ah/kg at low rates. The rate capability was improved by an aqueous carbon gel coating. The Ni rather than the Mn is the electrochemically active ion, the Mn remaining in the +4 oxidation state.

Stabilized vanadium oxides – high capacity cathodes

We have continued the evaluation of layered vanadium oxides stabilized by manganese. These have the double-sheet delta structure, and exhibit initial capacities exceeding 300 mAh/g (double that of lithium iron phosphate).

Conclusions: $LiFePO_4$ provides a low-cost highly reversible cathode but has a lower volumetric capacity than $LiCoO_2$. It is a good baseline system. The stabilized manganese oxides (*i.e.*, manganese-stabilized nickel oxides) show promise as the next-generation cathode. The vanadium oxides offer the greatest capacity, but at a lower voltage.

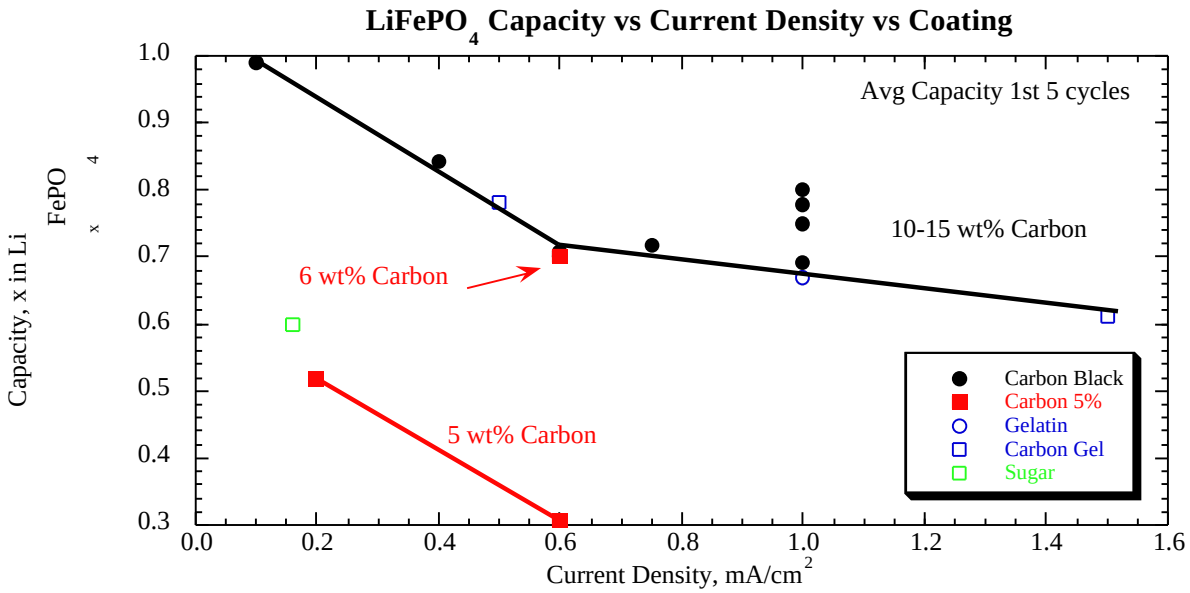

Figure 8. Room-temperature discharge capacity (mean value for the first five cycles) of $LiFePO_4$ as a function of current density and carbon coating procedure. Cathode loading is 20 to 80 mg/cm^2. Reaction of one Li per $FePO_4$ corresponds to a capacity of 170 mAh/g.

Novel Composite Anodes for Lithium-ion Batteries (**G.-A. Nazri and M. D. Curtis, University of Michigan, and T. Malinski, Ohio University)**

The primary objective is to develop a novel composite anode with higher energy and power density than the current carbonaceous anodes and with no intrinsic ICL, to improve the overall energy density, power capability, and safety of advanced Li batteries for transportation applications. Our approach is to prepare the composite anode using a simple and low-cost pre-lithiation process to stabilize the anode in contact with the electrolyte, and to overcome the problem of high first-cycle anode ICL in Li-ion batteries. This process will provide high-performance anodes with thermal and chemical stability for application in large Li batteries for transportation applications. Due to the stability of the prelithiated composite anode, a more-conventional and low-cost electrolyte also can be used. Further, the amount of Li in the anode can be tuned to allow the use of non-lithiated cathode materials, such as V_6O_{13}. Therefore, high-energy cathode materials can be coupled with the proposed composite anode.

We have developed two prelithiation processes to prepare anodes. The first process involves the prelithiation of anode powder before electrode fabrication, using a simple chemical process based on mechanochemistry of active materials with Li metal or with precursors containing Li, such as LiC_6 or highly lithiated alloys and compounds. This process allows us to not only prelithiate the anode powder but also tune the amount of Li in the anode powder by selecting the ratio of active anode powder to the amount of Li-containing precursors. The second process involves prelithaition of the anodes after fabrication, using constant current or a voltage pulse technique. In this method, we can control the degree of lithiation in the preformed anode by adjusting either the amount of charge or the anode voltage *vs*. a bulk metal anode.

We prelithiated a composite of natural graphite and tin oxide by a chemical process using mechanomilling techniques, and we successfully controlled the degree of prelithiation. In the first series of tests, the extent of prelithiation resulted in the complete reduction of the metal oxide to its metallic state. XRD, IR spectroscopy, and x-ray photoelectron (XPS) results confirmed the complete reduction of the oxide to its metallic state. In the second series of tests, we successfully extended the prelithiation process to proceed beyond the complete reduction of the oxide to form Li alloys. This type of synthesis was carried out for SnO, SnO_2, Sb_2O_3, and PbO materials. Electrochemical tests of these composites have shown no ICL due to oxide reduction, and a cycling test has indicated stable performance up to 700 cycles for a composite prelithiated SnO-LiC_6 anode. The anode capacity remained above 500 mAh/g after 500 deep cycles (100% depth of discharge).

In addition we have evaluated the over-lithiated composite anode against cathodes with no lithium content, particularly V_6O_{13}. Our preliminary results have shown that the over-lithiated SnO system can serve as an anode for vanadium oxide cathodes. A charge-discharge test of a Li-SnO/V_6O_{13} cell is in progress.

Future work will involve optimization of prelithaition process through mechnochemistry of alternative anodes to prepare high-energy and high-power electrodes for next-generation Li batteries.

Synthesis and Characterization of Cathode Materials (M. Doeff, LBNL)

$LiFePO_4$ has a theoretical capacity of 170 mAh/g at 3.45 V *vs*. Li but suffers from poor utilization in electrochemical cells due to low electronic conductivity and other factors. We have shown that reducing the particle size of a conventionally prepared sample of $LiFePO_4$ by planetary milling greatly improves utilization. Carbon-coated $LiFePO_4$ from the Université of Montreal also shows improved rate capability and good cycling. We have synthesized $LiFePO_4$ by several routes using low-cost precursors. A sol-gel route from iron nitrate is the most promising because it allows good control of particle size and allows addition of carbon during processing. We will evaluate sol-gel materials and make a go/no-go decision by the end of FY 2003.

The spinel $LiAl_{0.25}Mn_{1.75}O_{3.98}S_{0.02}$ was reported to have improved cycling stability on the 3V plateau. We synthesized $Li_{1.02}Al_{0.25}Mn_{1.75}O_{3.98}S_{0.02}$ and $Li_{1.02}Al_{0.25}Mn_{1.75}O_4$ by solid-state and sol-gel methods from acetates, nitrates and (optionally) Li_2S - see Fig. 9. We also received a sample from the Korean group who originally made this compound (by sol-gel) and reported on it. XRD, EDS and ^{7}Li MAS-NMR experiments indicated that sulfur is not present in the bulk of any of the samples. All materials showed low capacity (~ 90 mAh/g), poor rate capability, and a slow capacity fade when cycled on the 4V plateau. All materials lost capacity rapidly when cycled to 3V, although a donated sample showed a marked resistance to phase conversion at 3V. Because of this, the fade rate was slower than for samples made at LBNL. This is attributed to the unusual particle morphology of the donated material, which is a consequence of the presence of sulfur-containing compounds during firing. It is difficult to control the reaction of Li_2S with water and air during processing, so this effect could not be reproduced at LBNL. Because of the poor electrochemical properties of these materials and the irreproducibility of the synthesis technique, we recommended that work on this compound be dropped from the BATT Program.

Tunnel and O2 layered manganese oxides were made by ion-exchanging Na_xMnO_2 precursors. Tunnel-Li_xMnO_2 cycles stably and has excellent rate capability, but limited capacity. O2 layered compounds potentially have higher capacities but have been reported to undergo undesirable phase changes upon cycling, although no conversion to the spinel occurs. However, our cyclic voltammetry, galvanostatic cycling, and XRD experiments showed that no phase conversions of completely exchanged materials occur for at least 30 cycles. The capacity delivered upon galvanostatic cycling varies greatly with the substituents, with 150-180 mAh/g delivered when 11% of the Mn is substituted with Ni, Co, or Al. 11% substitution with Co or Zn reduces the capacity by nearly half, and Fe-containing materials appear to be especially rate-limited. A correlation of high capacity with the presence of some Li in an O3 environment (observed by NMR) and low capacity with the presence of some Li in a T2 environment has been noted. These environments are a consequence of stacking faults in the layers. The best materials will be chosen for further study in FY 2003. New materials with a potential for high energy density will also be examined.

Spinels discharged on the 4V plateau

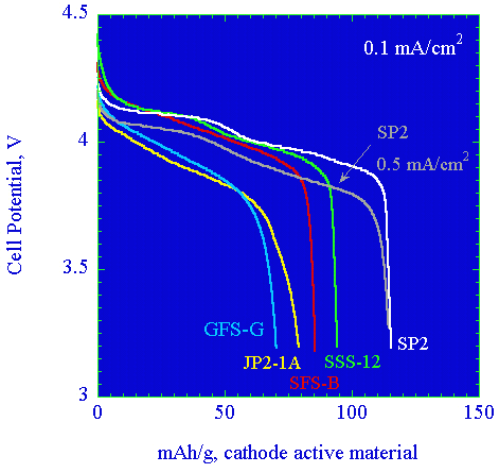

- Materials prepared by solid state methods better than sol-gel
- Materials with S slightly better
- All inferior to Merck spinel
- JP=sol-gel, Li_2S, made in-house
  GFS=sol-gel, no Li_2S
  SSS=solid state, Li_2S
  SFS=solid state, no Li_2S
  SP= Merck spinel
- All electrodes contain 8 wt% C

Li/1M $LiPF_6$, EC-DMC/JP2,SSS, SFS, GFS or SP, 8 wt% C cells discharged at 0.1 mA/cm^2

Figure 9. Performance of $Li_{1.02}Al_{0.25}Mn_{1.75}O_{3.98}S_{0.02}$ and $Li_{1.02}Al_{0.25}Mn_{1.75}O_4$ prepared by solid-state and sol-gel methods

Aluminum corrosion in Nonaqueous Electrolytes (T. Devine and J. Evans, LBNL)

To improve the corrosion resistance of current collectors, we are conducting experiments to characterize and understand Al corrosion behavior in candidate nonaqueous Li-ion battery electrolytes. We investigate Al corrosion behavior with methods: electrochemical DC polarization (ECDCP), electrochemical quartz crystal microbalance (EQCM), and scanning electron microscopy (SEM). By simultaneously conducting ECDCP and EQCM, we are able to concurrently measure, at a given Al potential, the current that crosses the Al/electrolyte interface and the change of Al electrode mass. Both the current and the mass change are related to the amount of corrosion that has occurred. In cases of uniform corrosion, knowing both the current and the mass change helps to identify the corrosion products. Knowing the corrosion products assists in identifying the corrosion mechanism. After corrosion testing, samples are examined by SEM for evidence of corrosion.

Figure 10 shows a representative set of results obtained in two different electrolytes. On the left-hand side are the results obtained in ATD Program Gen 2 electrolyte and on the right are the results obtained in EC+DMC with imide salt. For both sets of results, the upper figure presents the variation of current crossing the Al/electrolyte interface as a function of the applied potential, and the lower figure presents the increase in mass that accompanies the passage of current. The results of three voltage cycles are shown for each solution. The results for Gen 2 and 1M $LiN(CF_3SO_2)_2$/EC+DMC electrolytes represent the extremes detected in Al corrosion behavior. The sample tested in Gen 2 sustained no significant corrosion. As the Al potential is raised during the initial voltage cycle, the current increased, and a hysteresis occurred upon potential reversal. That the current during reversal is lower than that during the forward sweep is indicative of the formation of a protective film. The Al mass increase during the latter portion of the forward sweep is consistent with the formation of a protective film on the Al surface. Subsequent inspection of the sample by SEM confirmed the absence of significant corrosion.

In contrast, the results in the imide salt electrolyte indicate much larger corrosion currents and a positive hysteresis in the cyclic I-V curve, which is suggestive of localized corrosion. Although the currents are 100X larger in $LiN(CF_3SO_2)_2$ than in $LiPF_6$, the mass increase is only 10X larger. This is also consistent with Al corrosion. SEM confirmed severe pitting corrosion.

The results of tests conducted in other electrolytes are summarized in Table I. Collectively, the results indicate the following. First, some salts, e.g., $LiN(CF_3SO_2)_2$, are corrosive in most electrolytes. Second, other salts, *e.g.*, $LiPF_6$ and $LiBF_4$, are noncorrosive in most electrolytes. Third, still other salts, *e.g.*, $LiClO_4$, have corrosivities that depend on the identity of the solvent. Fourth, tests with mixtures of salts: $LiN(CF_3SO_2)_2$ + $LiPF_6$ and $LiN(CF_3SO_2)_2$ + $LiBF_4$ indicate the corrosivity of $LiN(CF_3SO_2)_2$ can be decreased. Because $LiN(CF_3SO_2)_2$ has high thermal and voltage stability, its use in Li-ion batteries offers distinct advantages. The use of $LiN(CF_3SO_2)_2$ has been precluded by its high corrosivity. The present results suggest that combinations of Li-ion salts might provide superior electrolytes that exhibit high stability and low corrosivity.

Future work will seek to understand the origin of Al corrosion resistance in electrolytes containing noncorrosive salts such as $LiPF_6$ and $LiBF_4$, and in electrolytes consisting of mixtures of salts of $LiN(CF_3SO_2)_2$ plus a critical concentration of a second salt (*e.g.*, $LiPF_6$, $LiBF_4$, *etc.* that imparts Al corrosion resistance. Other future work will involve long-term tests to determine the uniform and pitting corrosion rates of Al, along with extreme-value statistical analyses to predict the 15-year performance of Al current collectors in a large number of batteries.

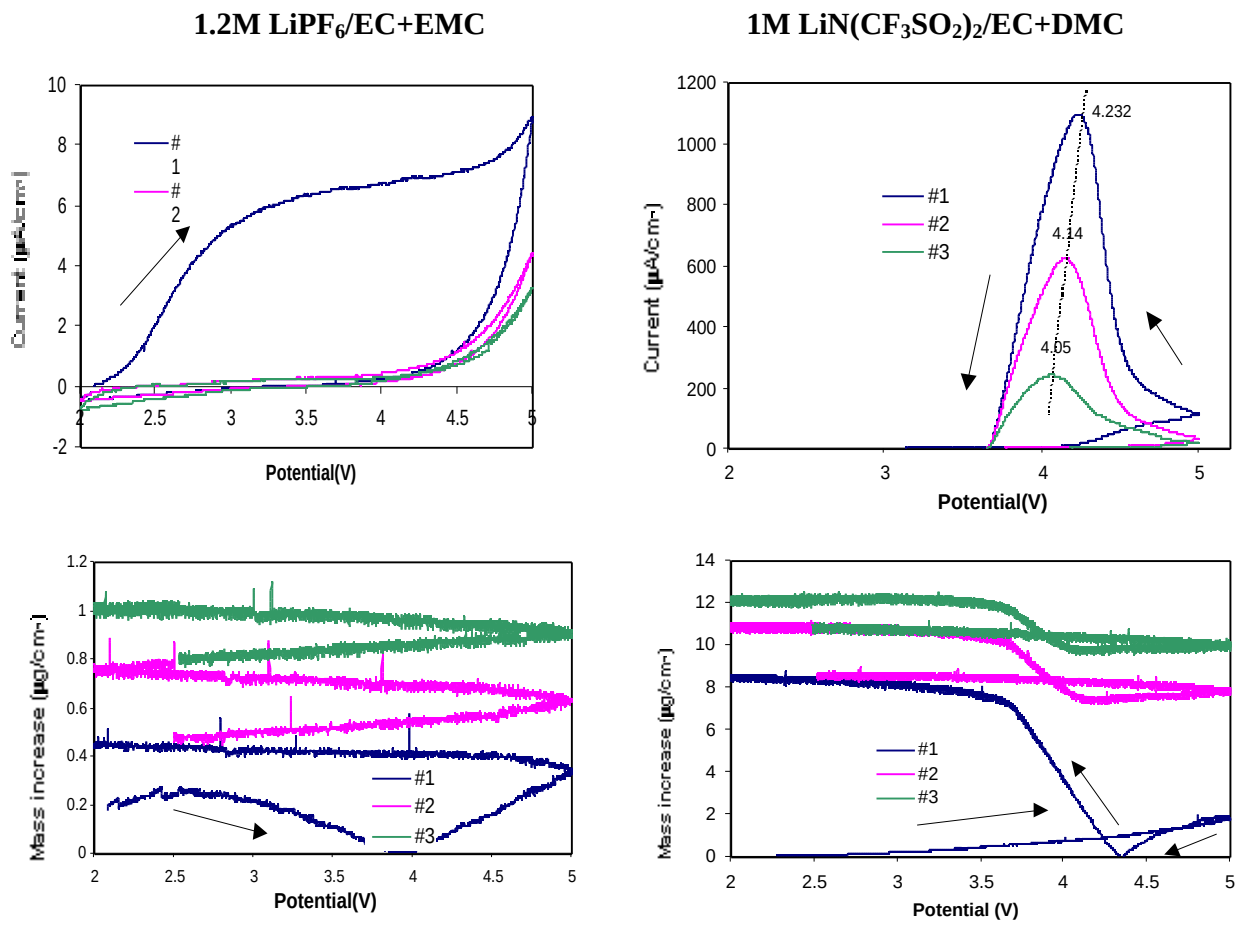

Figure 10. Representative set of results obtained in two different test solutions

Table I

Summary of Results

Salt	Is salt corrosive in PC?	Is salt corrosive in EC+DMC?
$LiN(CF_3SO_2)_2$	YES	YES
$LiCF_3SO_3$	YES	-
$LiC(CF_3SO_2)_3$	YES	-
$LiPF_6$	NO	NO
$LiBF_4$	NO	NO
50:50 $LiN(CF_3SO_2)_2$ + $LiPF_6$	NO	-
90:10 $LiN(CF_3SO_2)_2$ + $LiBF_4$	≈NO	-
$LiClO_4$	YES	NO

NMR and First-Principles Calculations of Two-Electron Redox Processes: The Layered Lithium Nickel Manganese Oxides (C. Grey, SUNY Stony Brook, and G. Ceder, MIT)

Layered cathode materials such as $Li[Li_{0.2}Cr_{0.4}Mn_{0.4}]O_2$ and $xLi(NiMn)_{0.5}O_2$. yLi_2MnO_3 have been discovered, wherein the oxidation/reduction processes involve multiple-electron redox processes. Our work is aimed at determining how these and related materials function in order to identify materials with improved capacities and cycling performances. The objectives and the experimental and computational approaches for this new research program were outlined and then illustrated by describing our preliminary results for the Li_2MnO_3-NiO system. NMR is used to probe local structure and to determine the local coordination environments and electronic structure, as a function of state of charge. First-principles calculations are used, for example, to determine the relative stability of different cation ordering schemes (Li, Mn, Ni) in the Li and transition metal (T.M.) layers, to help interpret NMR results, and to understand the effect of structure and dopants on the Ni^{2+}/Ni^{4+} couple.

Experimental results for two compounds, $Li[Ni_{0.5}Mn_{0.5}]O_2$ and $Li[Li_{1/9}Mn_{5/9}Ni_{3/9}]O_2$, were presented. ^{6}Li NMR results for both compounds clearly showed the presence of lithium ions in the lithium and transition metal (T. M.) layers of these layered materials (see Figure). The NMR results for $Li[Ni_{0.5}Mn_{0.5}]O_2$ are consistent with Ni^{2+} substitution into the lithium layers (see Fig. 11), as found in $LiNiO_2$. The lithium local environments in the T. M. layers resemble the lithium environments in the manganese layers of Li_2MnO_3 and can be represented by the local environment $Li(OMn)_{6-n}(ONi)_n$, where $n \geq 5$. These NMR results are in agreement with Mn and Ni EXAFS studies performed in collaboration with McBreen's group at BNL, which show that the manganese ions are located near a higher number of lithium ions than the nickel ions. Our preliminary 1st principles calculations indicate that Li local environments containing more Mn^{4+} ions are lower in energy than those surrounded by more Ni^{2+} ions and that Li doping in the T.M. layers reduces the tendency for Ni incorporation in the Li layers. Both the 1st principles calculations and XAS experiments show that the redox process involves nickel, the manganese ions remaining as Mn^{4+} during the 1st charge/discharge cycle at 4V.

The NMR results for both compounds clearly demonstrate that the lithium is removed from both the lithium layers and the T.M. layers on cycling (Fig. 11). The Li that remains in the structure at the end of charge is located in the lithium layers, near nickel. Calculations were performed in order to understand this phenomenon in more detail and showed that Li is removed from the Li and T.M. layers at similar potentials. The latter process is facilitated by Li vacancies in the T.M. layers. Li NMR showed that the Li ions return to the T.M. layers on discharging and that the process is reversible. The results should be contrasted with our earlier NMR study of $Li[Li_{0.2}Cr_{0.4}Mn_{0.4}]O_2$, where we showed that the lithium in the lithium layers of the chromium-rich domains was removed on charging, the lithium in the Li_2MnO_3 domains remaining in the structure.

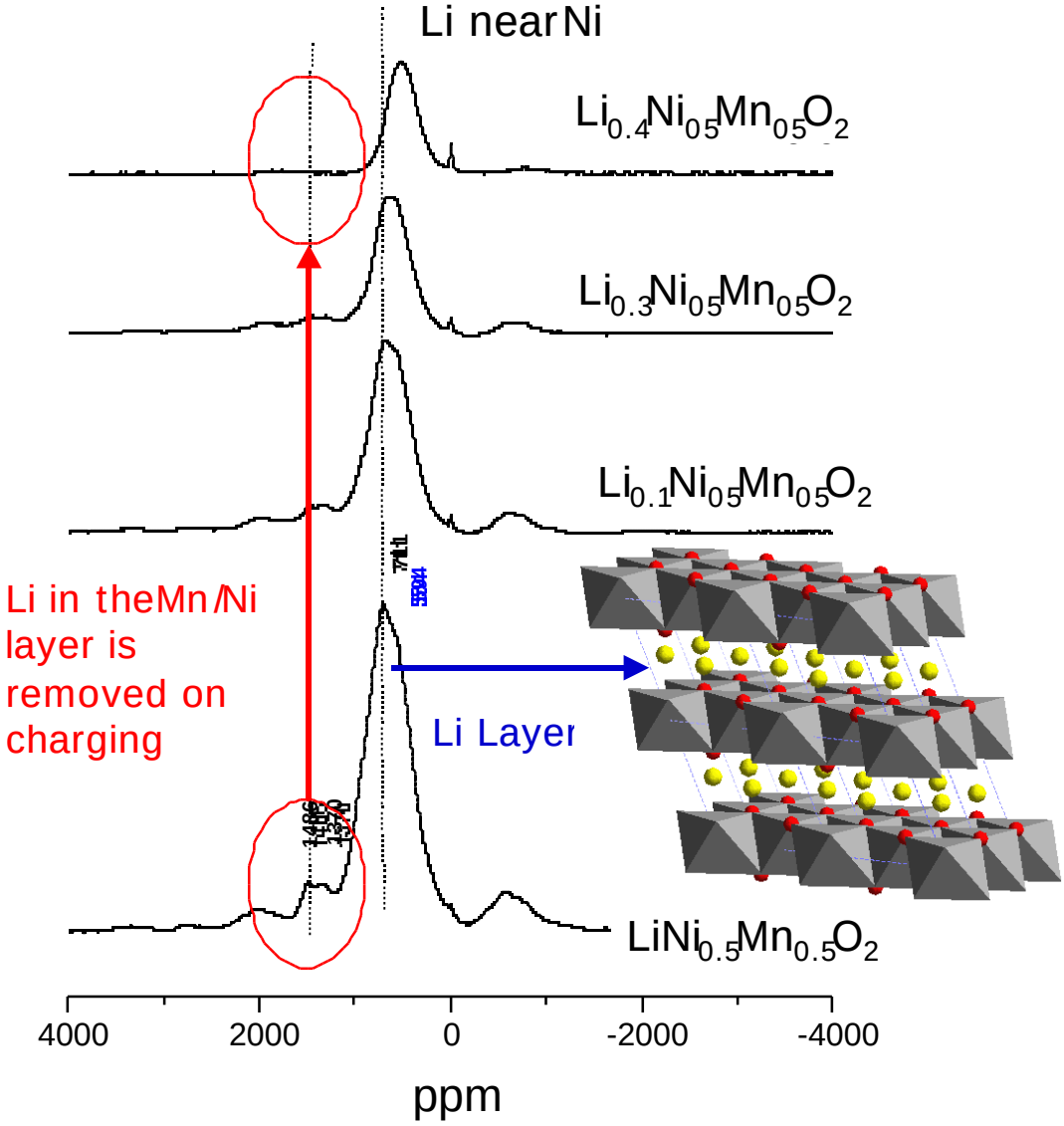

Figure 11. ^{6}Li MAS NMR of $LiNi_{0.5}Mn_{0.5}O_2$ as a function of state of charge shows that the Li environments in the T.M. layers (resonances at 1486 and 1370 ppm) are removed, along with some of the Li environments in the Li layers.

Polymer Electrolyte Design (N. Balsara and J. Kerr, LBNL)

The objective of this research task is to carry out the rational design of a polymer electrolyte to allow the practical development of high-performance batteries for transportation applications. The research approach is to synthesize model materials, measure parameters required for establishing models and use the models to guide development of the next generation of materials. As outlined in Fig. 12, this approach combines synthesis (Kerr), characterization (Balsara), theoretical modeling (Newman and Smith).

Polyethylene oxide (PEO) has remarkable conductivity and is an excellent starting point from the point of view of cost as well as practicality. However, the use of PEO has problems:

- Dendrite growth with lithium metal is difficult to control.
- Room-temperature operation is not possible with ethylene-oxide based polymers. Polymers based on other solvating groups such as trimethylene oxide (TMO) and butanediol (BDO) are under study. The cost of TMO units has recently dropped to $0.59/lb from $26/lb.
- Cells exhibit poor stability, especially at electrode interfaces. Four-volt cell operation is desirable and demands the use of multilayer polymer electrolytes with different chemical, electrochemical and mechanical properties in order to achieve high energy and power densities.

We report the following accomplishments:

- TMO polymers improve low-temperature conductivity but have little effect on the Arrhenius barrier to Li-ion mobility. The nature of the barrier to Li-ion motion is unresolved.
- Salt concentration gradients contribute to interfacial impedances due to phase changes close to the electrodes, and contribute to capacity fade. Lower dependence of Tg values of TMO polymers with salt concentration gives lower interfacial impedance and provides the prospect of better capacity behavior with cathodes.
- Single-ion conductors offer a solution to problems caused by concentration gradients.
- Nanoparticle fillers help mechanical properties and restrain dendrite growth. No benefit is observed with conductivity using LiTFSI salt.
- Cross-linking improves mechanical properties and lithium cycling (dendrites). The uniformity of the curing process and cross-link density are critical.

Our future plans include the following tasks:

- Continue work on barriers to ion mobility. Synthesize and characterize appropriate polymers. Physical characterization (Balsara, Kostecki, Khan) and modeling (Smith).
- Continue development of curing chemistry and filler addition to provide uniform membrane properties for scale-up. Match with models of cell performance and dendrite growth (Newman).
- Continue work on particle-polymer interactions for electrode structure design.
- Study modifications of electrode surfaces. Vacuum deposition of Li, chemical/physical reactions at surfaces (synergies with organic LED work for solid-state lighting).
- Develop single-ion conductor ionomers for optimum composite electrode structures. (Ionomer work applicable to batteries, fuel cells, and OLEDs).

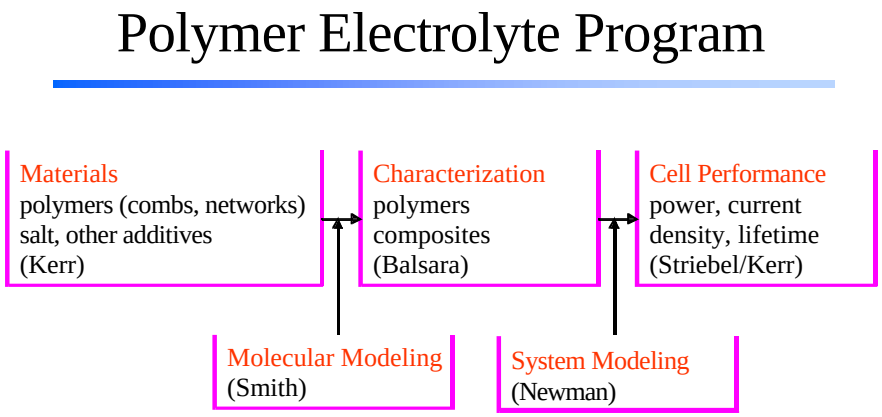

Figure 12. Polymer electrolyte research structure

Composite Polymer Electrolytes (S. Khan, P. Fedkiw, North Carolina State University; and G. Baker, Michigan State University)

The ultimate objectives of this task are to develop composite polymer electrolytes that are low-cost, have high conductivities, impart electrode-electrolyte interfacial stability, and yield long cycle life. Our approach is to use surface-functionalized fumed silica fillers in BATT-baseline systems to determine the effects of filler type and concentration on interfacial stability and cell cycling. We intend to correlate these electrochemical characteristics with mechanical properties and materials chemistry. Data to be collected include modulus, ionic conductivity, Li cycling efficiency, Li-electrolyte interfacial resistance, and full-cell cycling capacity using 3-V cathodes.

We have systematically investigated the effect of adding fumed silica into low-molecular-weight polymers. Composite electrolytes are obtained by dispersing fumed silica particulates into a liquid electrolyte that is composed of poly(ethyleneglycol)dimethylether (Mw=250) + LiTFSI. The self-assembly of the fumed silica forms three-dimensional continuous networks, which originate from hydrophobic interactions, solvation forces and/or hydrogen bonding of the surface groups on the silica. These composite electrolytes exhibit desirable mechanical properties characteristic of solids (elastic modulus G' in excess of 10^5 Pa), yet have the processability of liquids and display conductivities rivaling liquid electrolytes ($\approx 10^{-3}$ S/cm at 25°C). The transport and rheological properties of these composite electrolytes are decoupled. The composite electrolytes also demonstrate the desirable property of suppressing Li dendrite growth due to the rigidity and immobility of the electrolyte structure. The Li/electrolyte interfacial resistance for composite electrolytes is less than that for the corresponding base-liquid electrolyte, and the charge-discharge cycle performance, electrochemical efficiency, rate capabilities, and self-discharge performance for the Li/V_6O_{13} cell are significantly improved.

We have also investigated the effect of adding fumed silica into baseline high-molecular-weight polymer. Composite polymer electrolytes are obtained by dispersing fumed silica particulates into poly(ethylene oxide) (Mw=200K and 600K) + LiTFSI. The fumed silica forms a network structure and provides mechanical support even when the PEO has melted. In crystalline polymer electrolytes, adding fillers increases the conductivity as the crystallinity always decreases. In amorphous polymer electrolytes, adding fillers decreases conductivity according to a volume-dilution effect.

We also investigated a mixed polymer system (Fig. 13). Fumed silica in PEO mixtures (PEO (600K):PEGdm(250) (1:1)) exhibit enhanced conductivity and elastic-like properties. These mixtures are promising candidate electrolyte and are under investigation.

Conductivity/Rheology of PEO Mixtures

PEGdM(250):PEO(600K)=1:1 (mass); LiTFSI(Li:O=1:20)

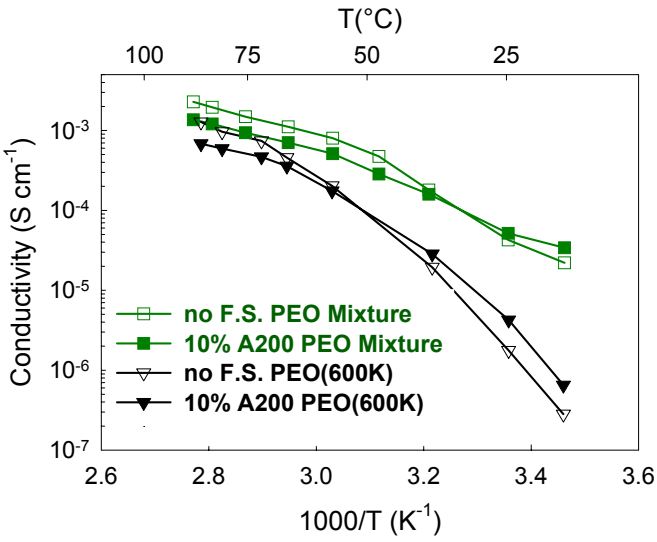

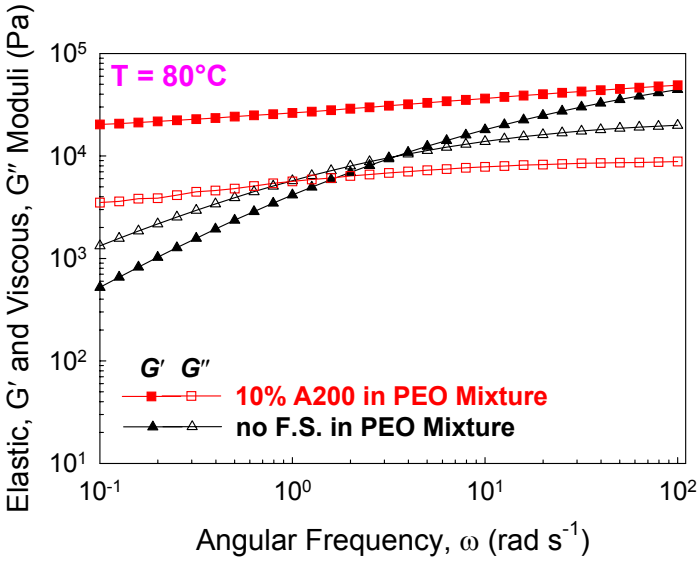

- Adding low-MW PEO increases conductivity
- PEO mixture with **10% A200** exhibits elastic-like properties at 80°C even with the addition of low-MW PEGdm(250)

New Battery Electrolytes Based on Oligomeric Lithium Bis((perfluoroalkyl)sulfonyl)imide Salts (D. DesMarteau and S. Creager, Clemson University)

Synthetic schemes for making oligomeric imide salts via linkage of bis(sulfonyl fluoride) monomers with bis(trimethylsilyl-activiated sulfonamide) monomers have been developed and are being used to prepare a series of dimeric and oligomeric Li salts for use as Li/polymer battery electrolytes. Figure 14 presents details on the synthesis of a dimeric imide-based Li salt. Similar methods have been used to prepare dimers with perfluoroethyl, butyl, hexyl, and octyl chains linking imide anions together. All of these dimers, and several other related Li salts made using similar methods, have been characterized regarding their ionic conductivity in polyether host matrices.

Figure 15 presents some representative data on ionic conductivity vs. reciprocal temperature for a series of dimeric imide Li salts in a high-MW PEO host and also in a lower-MW crosslinked PEO host. The trends in conductivity observed in the high-MW PEO host are similar to those we have previously reported, i.e., within the series of dianionic salts the ionic conductivity increases with increasing fluorine content in the salts. This effect is thought to reflect the fact that the negative charge is more delocalized in the more highly fluorinated salts, which diminishes ion pairing and generates more free ions to transport charge. A similar effect is noted in the electrolyte prepared using a crosslinked PEG host, except that in all cases the conductivities are lower than for the crosslinked than for the non-crosslinked electrolyte. This may reflect the fact that the crosslinked electrolytes have been too highly crosslinked, to the point that the matrix is impeding ion transport. It may also be the case that the chemical nature of the crosslinks (they are urethane linkages) causes them to serve as traps for ions.

Future work on this project will be pursued along the following directions:

- Synthesize ionenes with variable linkages, chain lengths.
- Measure transference numbers for SPEs fabricated using new imide salts.
- Prepare and test SPEs with variable degrees of cross-linking.
- Explore the use of plasticizers (e.g. PEGDME) with cross-linked SPEs

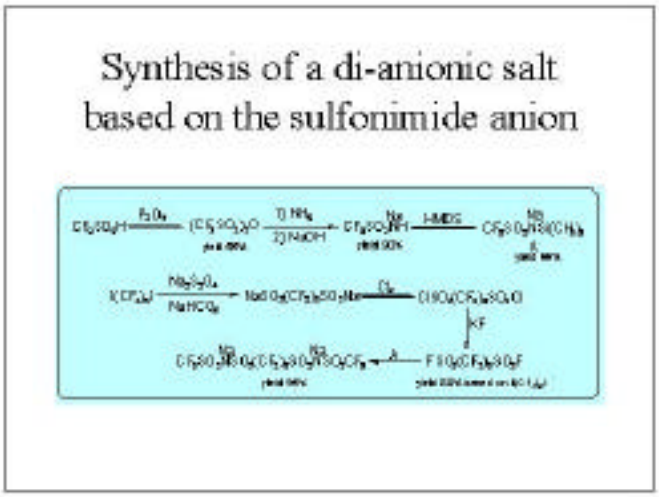

Figure 14. Details of the synthesis of a dimeric imide-based Li salt

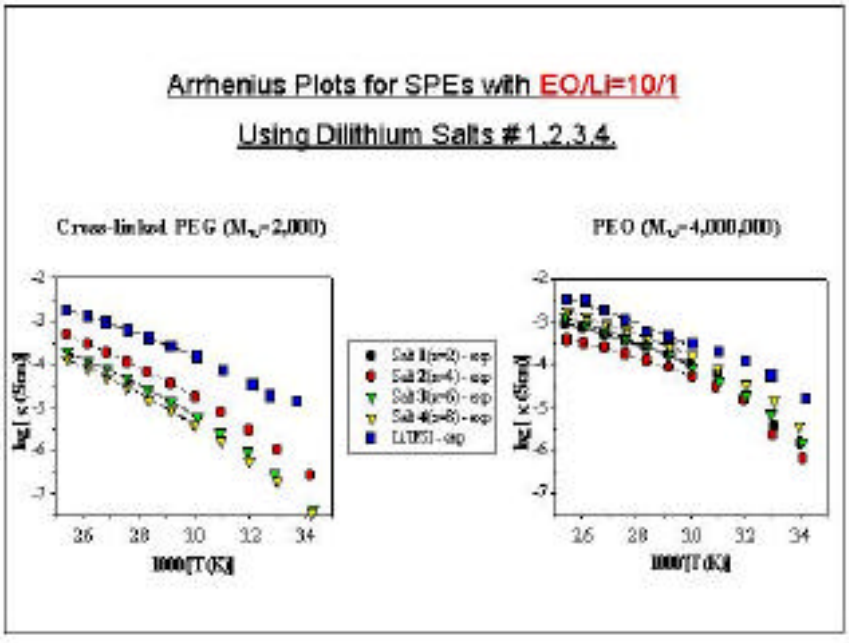

Figure 15. Ionic conductivity vs. reciprocal temperature for a series of dimeric imide Li salts in high-MW PEO and in lower-MW crosslinked PEO.

Influence of Polymer-Ion Interactions and Polymer Conformational Properties on Transport in Polyether-based Solid Polymer Electrolytes (G. Smith and O. Borodin, University of Utah)

The objectives of this task are to understand the influence of polymer host properties on structure and transport in solid polymer electrolytes (SPEs) through atomistic simulation studies of: (*i*) the influence of polymer-cation interactions on the structure and transport properties of SPEs, (*ii*) the influence of polymer segmental dynamics and torsional barriers on the structure and transport properties of SPEs, and (*iii*) the influence of polyether architecture (PEO, POM, PPO, POM3, copolymers) on SPE structure and transport properties.

Two systems are currently under study:

PEO (MW=2380)-$LiBF_4$

1. Li^+-PEO interactions and conformational energetics parametrized from quantum chemistry

2. Investigation of the influence of increased and decreased strength of Li^+-PEO interactions on ion clustering, dynamics, and conductivity (see Fig. 16)

3. Investigation of increased PEO torsional barriers on ion clustering, dynamics, and conductivity

PEO and POM-$LiBF_4$, EO:Li=15:1

1. Li^+-polymer interactions and conformational energetics parametrized from quantum chemistry

2. Comparison of ion clustering, dynamics, and conductivity

Work is progress includes: (*i*) additional parametric studies of the influence of conformational energetic and ether-Li^+ interactions on structure and transport in SPEs, (*ii*) force field parametrization and MD simulations of poly(propylene oxide)-$LiBF_4$, and poly(trimethylene oxide)-$LiBF_4$, and (*iii*) investigation of OE-OM_3 copolymers (linear, comb-branch) as candidates for a polymer host for SPEs with improved transport properties.

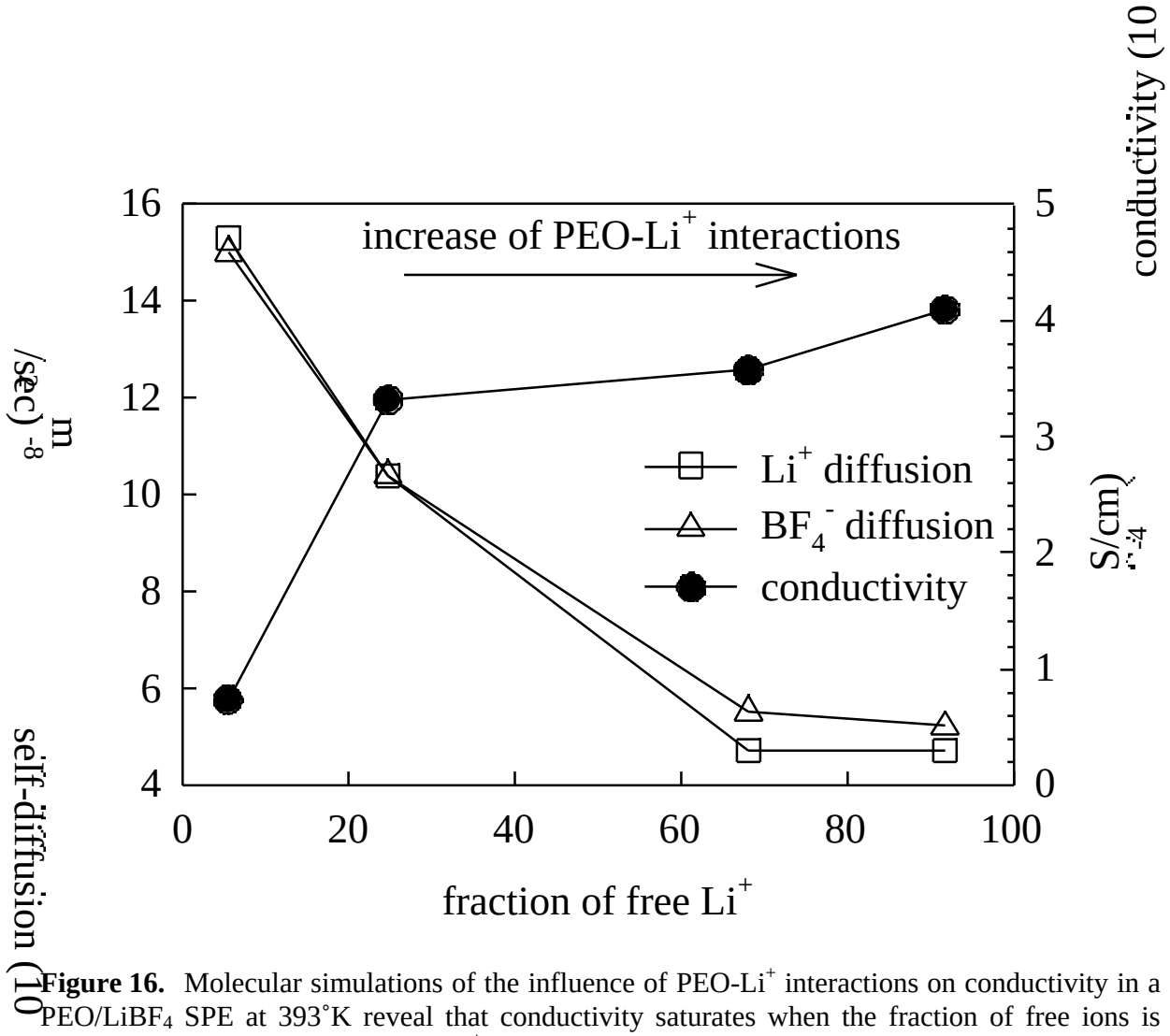

Figure 16. Molecular simulations of the influence of PEO-Li^+ interactions on conductivity in a PEO/$LiBF_4$ SPE at 393˚K reveal that conductivity saturates when the fraction of free ions is about 30 % due to too-strong PEO-Li^+ attraction resulting in decreased ion mobility.

Electrolyte Additives (J. Kerr and K. Kinoshita, LBNL)

This task addresses several issues related to liquid electrolytes

Chemical Reactions in Lithium Ion Battery Electrolytes

Reactions of the bulk electrolyte in the absence of electrodes. Lewis acid salts such as $LiPF_6$ catalyze ring-opening polymerization of EC to yield PEO-like and polyether carbonate polymers, as well as CO_2. (Fig. 17)

Reactions of the electrolyte components at the electrodes. In addition to reactions of the known components of the electrolytes (EC, DMC, DEC, *etc*.), the products of the chemical reactions that form in the bulk of the electrolyte are also electroactive. CO_2 is reduced to CO, carbonate, formate, and oxalate while PEO-like polymers are oxidized at high-voltage cathodes to yield acid and other species that promote further polymerization, cross-linking, and poor transport properties within the electrode structures.

Effect of reactions on battery performance. The reaction scheme shown in Fig. 17 provides a reasonable rationalization of many observations of Li-ion battery performance reported in the literature, in the ATD Program, and in the BATT program. The reaction scheme shows that the electrolyte stability is precariously balanced and can be destabilized by removal of CO_2. Reduction of CO_2 at the anode to CO, carbonate , oxalate, and formate destabilizes the system.

Consequences of Reactions in Composite Electrodes

In both composite anodes and cathodes, chemical reactions occur that can generate polymeric material in confined volumes between the electrode particles. Such a situation leads to decreased transport properties of the Li ions within the electrodes, leading to increased impedance and cell power loss. These effects can be mitigated by control of the electrode particle size and surface properties.

Additives: Pyridine and Vinylene Carbonate

One can prevent the chemistry outlined in Fig. 17 by removing the EC. However, doing so prevents use of carbon anodes. Pyridine is a Lewis base and intercepts the damaging PF_5 thereby preventing polymerization reactions, however pyridine undergoes undesirable reactions.

Vinylene carbonate may also intercept PF_5 but it is also known to be reduced at the anode. It is thought that the VC forms a film that inhibits undesirable reactions. However, this film must be selective for Li ions while blocking reduction of CO_2, a most remarkable selectivity. Use of VC in this manner to extend calendar and cycle life also runs the risk that the additive may become exhausted before the end of battery life. It is also possible that VC acts as a redox catalyst.

Redox catalysis additives and CO_2/carbonate reduction

Redox catalysis of the reduction of EC, DMC, and CO_2 provides unique and useful insight into anode electrochemistry and surface film formation. These aspects will be studied in depth in the coming months.

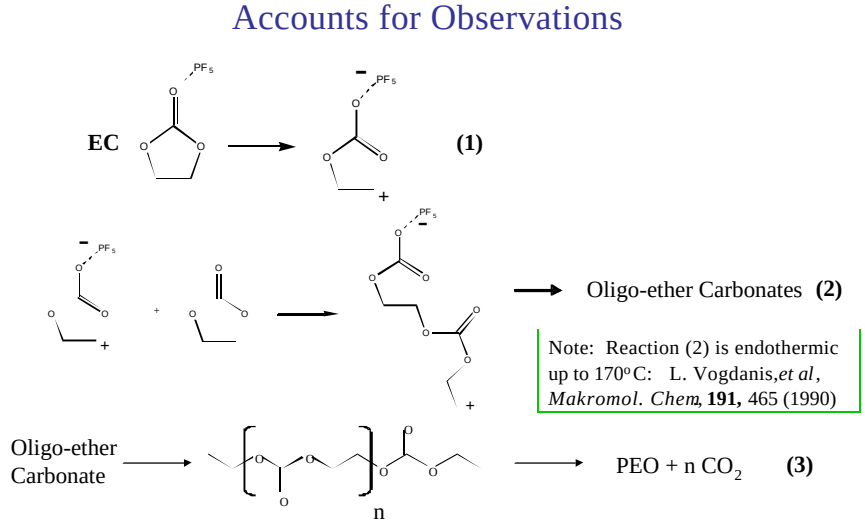

Figure 17. Scheme for Li-ion battery electrolyte reactions

Electrode Surface Layers (R. Kostecki and F. McLarnon, LBNL)

We used Raman microscopy and atomic force microscopy (AFM) to monitor and understand the effect of structural changes which occur in graphitic materials upon extensive cycling at elevated temperatures. By combining these two methods of surface analysis we can evaluate the surface and near-surface changes resulting from exposure of the graphitic electrodes to stresses that arise from numerous Li intercalation/deintercalation cycles and elevated temperatures.

The electrochemical intercalation of Li into carbonaceous materials has been studied extensively for use in Li-ion battery anodes. Raman spectroscopy is one of the preferred methods of analysis of graphitic structures, because it provides structural information second only to XRD. Although this technique is suited to only near-surface studies because of the high optical extinction coefficient of carbon, it is extremely sensitive to changes that disrupt the translational symmetry of graphite basal planes.

The synthetic graphite electrodes (MAG-10, Hitachi Chemical) which are used in the ATD Program Gen 2 Li-ion cells were cycled in a small 100 mAh cell manufactured by Quallion (cell ID Q0120V) and two 15-mAh lab-size pouch cells (PG04, PG13). The $LiNi_{0.8}Co_{0.15}Al_{0.05}O_2$ Gen 2 composite cathode was used in all cells, and was combined with $LiPF_6$-EC-DEC electrolyte in cells Q0120V and PG04 and LP40 electrolyte in cell PG13. The cells were charged and discharged ~400 times at the C/2 rate and 100% DOD between 3.0 and 4.1 V at ambient temperature (Q0120V, PG04) and at 60°C (PG13). All cells exhibited capacity loss at the end of cycling which was measured at C/2 rates, *i.e*., 13%, 33%, and 65% for Q0120V, PG04, and PG13 respectively - see Fig. 1.

Figure 18 shows Raman images of the integrated intensity ratio of D/G carbon Raman bands collected from a 40 x 60 μm area with 0.7 μm resolution. The G-band which is located at 1580 cm^{-1} arises from the first-order scattering associated with the in-plane E_{2g} mode, whereas the D-band is associated with the break of symmetry occurring at the edges of graphite sheets. In general, the more edges or defects that are present in the graphite lattice, the more intense this band becomes. The integrated intensity ratio of D/G bands, which is inversely proportional to the size of microparticles and increases with carbon disorder, is often used to evaluate carbon structures.

The D/G ratio on the Raman maps shown in Fig.18 is represented by different shades of gray. The lighter is the shade of gray on the image, the more graphitic is the electrode structure. The Raman images in Fig. 18 reveal that in general, the graphite undergoes gradual structural degradation upon cycling. However, severe structural disorder was observed in the anode from the cell which was cycled at 60°C. Interestingly, the structural degradation of graphite did not occur uniformly on the electrode surfaces. Even in the anode which shows substantial damage on its surface (PG13 cell), one can still identify regions which consist of undisturbed graphite. Distortions in the graphite structure can create a barrier for Li ion diffusion during the intercalation-deintercalation process, contributing to the electrode impedance rise. On the other hand, structural degradation of the graphite led to an increased anode surface reactivity *vs*. the electrolyte, and the formation of solid electrolyte interphase (SEI) layers. A thick layer of inorganic products from side reactions, signaled by Raman bands at 1000-1100 cm^{-1} that are characteristic for carbonates and phosphates, was observed on the disordered part of the carbon anode. The presence of these products suggests that structural changes in the electrode surface greatly affected the composition of the SEI layer and caused a permanent shift in Li inventory in the tested cells.

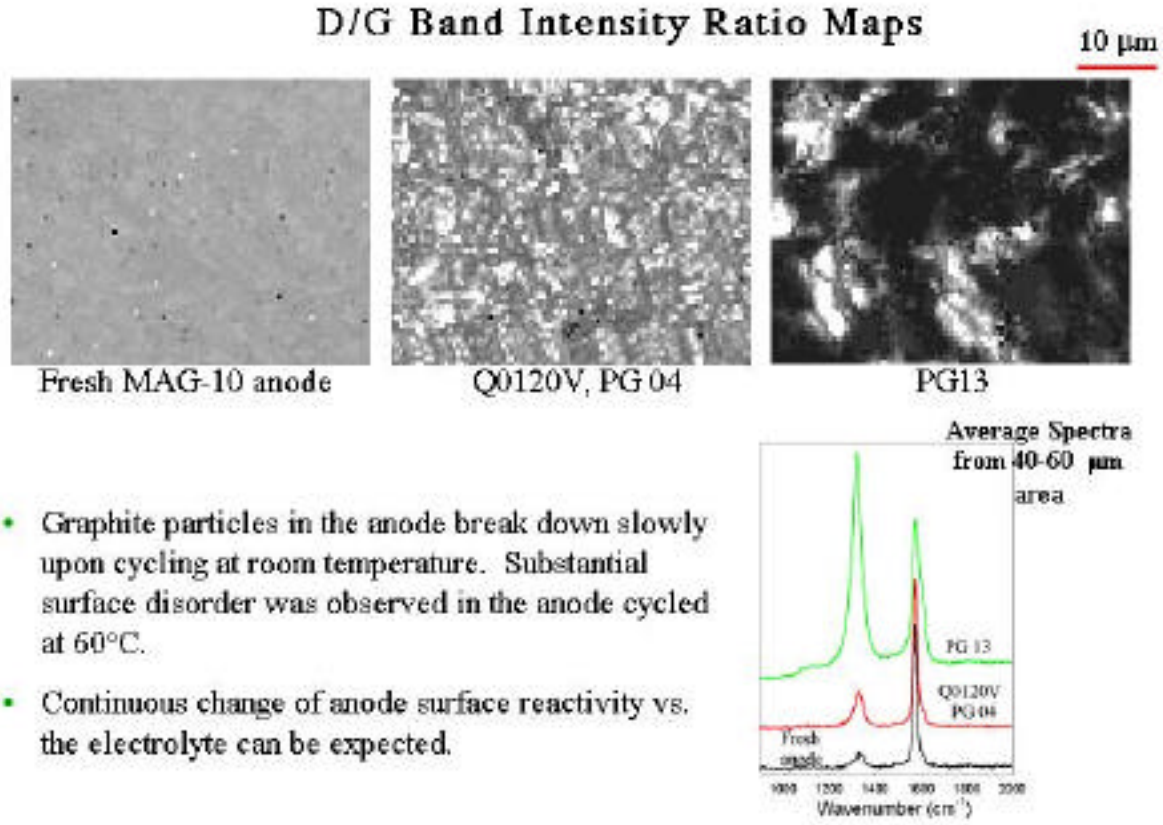

Figure 18. Surface structure of BATT Program anodes

Battery Materials: Structure and Characterization (J. McBreen, Brookhaven National Laboratory)

The objective of this task is to develop and apply advanced diagnostic techniques, with sensitivity to bulk and surface processes, to monitor degradation processes in Li-ion batteries. These techniques are also being used to elucidate properties of starting materials that determine performance and stability of $LiMn_2O_4$ and other low-cost cathode materials with higher capacity ($LiFePO_4$ and $LiNi_xMn_{1-x}O_2$). We use a combination of *in situ* and *ex situ* x-ray absorption spectroscopy (XAS) and XRD to study bulk processes in electrodes. We also use *ex situ* soft x-ray XAS in both the electron yield and fluorescence mode to distinguish between surface and bulk processes on electrodes. In the soft x-ray regime from 500-1000 eV the escape depth for the Auger electrons is about 50Å, and the sampling depth for the fluorescent signals is about 3000 Å. Thus the former probes close to the surface whereas the latter probes the bulk.

Extensive *in situ* XRD on $LiMn_2O_4$ that in the 4.1 V region indicated that there are two first-order phase transitions with three cubic phases. The studies of $LiMn_2O_4$ indicate that the cycle life and stability of $LiMn_2O_4$ can be greatly improved by use of excess Li stoichiometry, elimination of oxygen deficiency, and by using stable electrolytes that do not generate acidic species in the cell. Excess Li stoichiometry increases the range of lattice constants for all three phases and yields pseudo single-phase behavior. Increasing oxygen deficiency promotes the conversion of the cubic spinel to a tetragonal phase at low temperature. The transition temperature, the transition kinetics, and the amount of the spinel converted to the tetragonal phase increases with increasing oxygen deficiency.

Both *in situ* XRD and XAS reveal the presence of a first-order phase transition during charge ($LiFePO_4 \rightarrow FePO_4$). Principal-component analysis of the Fe near edge XAS (see Fig. 19) clearly show that a maximum of two components (indicating the presence of only two distinct phases) can account for the XAS data at all states of charge. *In situ* XRD of $LiNi_{0.5}Mn_{0.5}O_2$ indicates that it has the $R\bar{3}m$ structure. During charge the H1 phase is converted to the H2 phase, accompanied by an elongation of the c-axis and a contraction of the a-axis. Unlike other materials with the $R\bar{3}m$ structure (LiNiO2 and $LiNi_{0.8}Co_{0.2}O_2$) there is no conversion to the H3 phase, even at 4.6 V. However, $LiNi_{0.3}Mn_{0.7}O_2$ did show formation of the H3 phase, indicating that stable operation requires the $LiNi_{0.5}Mn_{0.5}O_2$ composition.

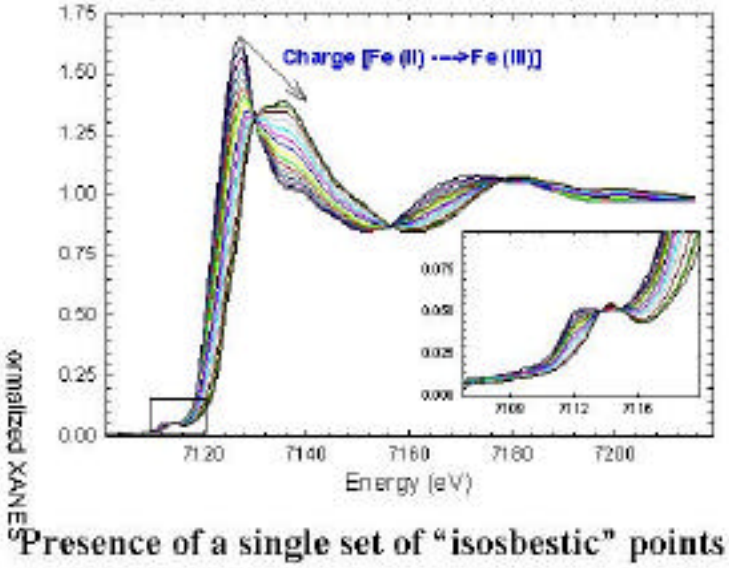

Figure 19. *In situ* Fe K-edge XAS of $LiFePO_4$

Interfacial and Reactivity Studies (P. Ross, LBNL)

Solvent Reduction

The reduction potentials of five organic carbonates commonly employed in Li battery electrolytes, ethylene carbonate (EC), propylene carbonate (PC), diethyl carbonate (DEC), dimethyl carbonate (DMC), and vinylene carbonate (VC) were determined by cyclic voltammetry using inert (Au or glassy carbon) electrodes in THF/$LiClO_4$ supporting electrolyte. The reduction potentials for all five organic carbonates were above 1 V (*vs*. Li/Li^+). PC reduction was observed to have a significant kinetic hindrance. The measured reduction potentials for EC, DEC, and PC were consistent with thermodynamic values calculated using density functional theory (DFT) assuming one-electron reduction to the radical anion. The experimental values for VC and DMC were, however, much more positive than the calculated values, which we attribute to different reaction pathways. The role of VC as an additive in a PC-based electrolyte was investigated using conventional constant-current cycling combined with *ex situ* infrared spectroscopy and *in situ* atomic force microscopy (AFM). We confirmed stable cycling of a commercial Li-ion battery carbon anode in a PC-based electrolyte with 5 mol % VC added. The preferential reduction of VC and the SEI layer formation therefrom appears to inhibit PC co-intercalation and subsequent graphite exfoliation.

Solvent Oxidation

The electrochemical oxidation of alkylcarbonate solvents and/or additives of interest in Li-ion batteries was studied using a combination of the classical rotating ring disk electrode (RRDE) method and *in situ* infrared reflection absorption spectroscopy (IRRAS). The oxidation potentials predicted by density functional theory (DFT) assuming one-electron oxidation to the radical cation for the common Li-ion battery solvents, EC, DEC, and DMC were all near 5.5 V (+/- 0.1 V), well above the cut-off potential of 4.2 V normally used in Li-ion batteries. DFT predicts that decomposition of the radical cation producing CO_2 is nearly adiabatic for the cyclic carbonates (EC and PC). The RRDE results for a standard Li-ion battery electrolyte EC:DMC/1M $LiPF_6$ is shown in Fig. 20. The disk and ring electrode are both Pt. The result shown is for a ring potential of 2 V (*vs*. Li/Li^+), but scanning the ring potential while holding the disk at 5.5 V indicated the ring current has a peak near this potential, indicating the ring current most probably corresponds to reduction of CO_2 produced at the disk electrode at potentials above ca. 5.2 V. The *in situ* IRRAS experiments were consistent with this conclusion, with the IR peak for CO_2 in solution observed when the electrode potential was increased above *ca*. 5.2 V. DFT predicted that the oxidation potentials of the unsaturated cyclic carbonates vinylene carbonate and catechol carbonate, that are proposed electrolyte additives, have an oxidation potential that is *ca*. 1 V lower, 4.1 (+/- 0.1 V), and with CO not CO_2 as the energetically favored decomposition product. The *in situ* IRRAS experiments were consistent with this prediction, with the vinylene C-H stretch disappearing above *ca*. 4.2 V and a band characteristic of CO appearing. The experimental results are thus in complete agreement with the predictions of DFT, and *vise versa*.

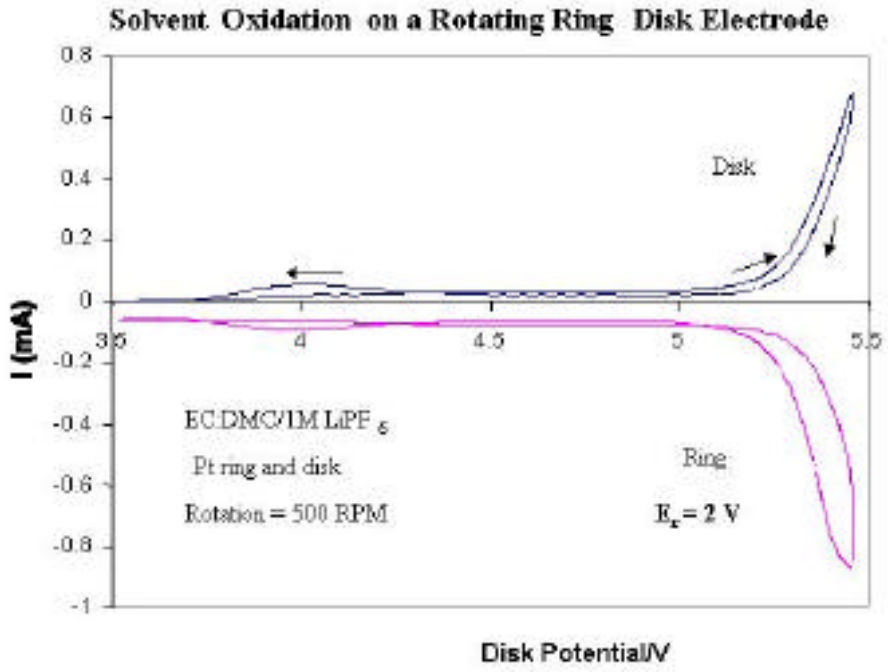

Figure 20. RRDE results for a standard Li-ion battery electrolyte EC:DMC/1M $LiPF_6$

Cathode Material Studies Using ^{7}Li NMR (E. Cairns, LBNL)

The objectives of this task are to directly observe Li in BATT Program cathodes, to characterize the local environment of Li (atomic and electronic), to determine the changes in the Li environment with cycling (identify failure mechanisms), and to use the above information for designing improved materials. Electrode materials studied include the following:

$LiM_xMn_{2-x}O_4$ Spinels	Li Gel
$Li_{0.47}M_xMn_{1-x}O_2$ Tunnel	Li Polymer
$Li_y[M_{0.11}Mn_{0.89}]O_2$ Layered	Li P or Li Gel
$LiAl_{0.05}Ni_{0.80}Co_{0.15}O_2$	Li Ion (ATD Program Gen 2)
$LiFePO_4$, $Li(Fe,Mn)PO_4$	Li Gel
$LiAl_xMn_{2-x}(O_{4-y}S_y)$	Li Gel

Results and conclusions from studies of these materials are provided below:

Layered $Li_y[M_{0.11}Mn_{0.89}]O_2$

- ^{7}Li NMR spectroscopy is very useful in determining the structure of $Li_y[M_{0.11}Mn_{0.89}]O_2$.
- The materials can be categorized into three different combinations of Li environments based on the differences in the NMR spectra, and this correlates with cell cycling performance.
- Depending on the metal substituent, three discrete resonances are observed at 700, 300, and 100 ppm, and these can be assigned to O2, T2, and O3 type local environments, respectively.
- No ordering between the Mn and the substituent atoms in the T.M. layer is observed
- No Li cation substitution in the T.M. layer is observed.
- The electrodes which contain the T2 environment (resonance at 300 ppm) show lower capacity.

$LiMPO_4$-based materials

- ^{7}Li spectra of $LiFePO_4$ are characterized by a broad spinning sideband manifold, and an isotropic linewidth dominated by chemical shift dispersion
- The shifts for $LiMPO_4$ are readily explained by the STH interaction, taking into account the Cs metal site symmetry
- Spectra of $Li(Fe,Mn)PO_4$ indicate a homogeneous distribution of Mn and Fe ions; the NMR shift and linewidth vary systematically with Mn content
- These results form the basis for interpretation of spectra from cycled electrodes

Gen 2 $LiAl_{0.05}Co_{0.15}Ni_{0.80}O_2$

- Damage resulting from storage and cycling results in loss of Li NMR signal from the $LiNiO_2$ sites (Fig. 21)
- The Li in the $LiCoO_2$ sites is retained
- Further work will identify the cause of this loss

$LiAl_xMn_{2-x}(O_{4-y}S_y)$

- No evidence is seen for incorporation of S into the bulk of the material
- Evidently, the S affects only the particle morphology

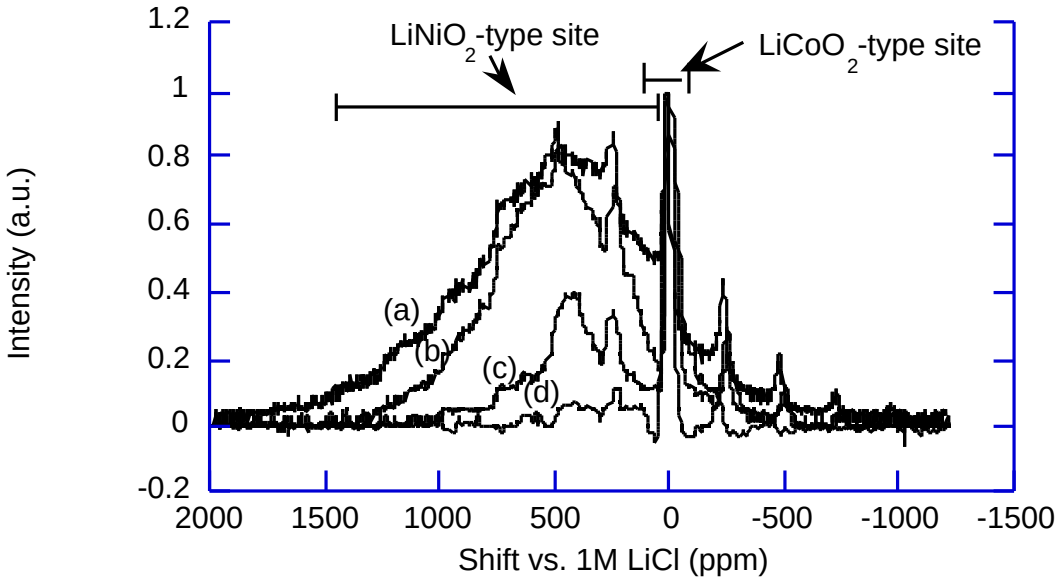

Figure 21. NMR Spectra for Gen 2 $LiAl_{0.05}Co_{0.15}Ni_{0.80}O_2$. (a) = Fresh electrode, (b) = # I116 Cycled once, (c) = # A212 Stored, lost 24% power, (d) = #PG13 Cycled 140 times, lost capacity.

Improved Electrochemical Models (J. Newman, LBNL)

We modeled side reactions in battery systems as they influenced the measurement of transport measurements by the galvanostatic polarization method. We find that diffusion coefficient and conductivity measurements are negligibly influenced, but the concentration-cell measurements, which directly influence the transference number and activity coefficients, can lead to errors at low concentrations. However, if side reactions are small, reliable results are still obtained. An additional transition-time measurement was run and simulated to reveal the reliability of the other, already measured properties as a function of concentration.

Molecular dynamics was used to simulate the behavior of $LiPF_6$, a common battery electrolyte salt, in solution in propylene carbonate, ethylene carbonate, and methyl ethyl carbonate. This is based on pairwise potential functions, whose refinement should lead to better agreement with experimentally measured diffusion coefficients. The calculation methods developed here can apply to solutions with any number of species and should represent the wave of the future in this area. Results suggest that the decrease in conductivity and increase in viscosity with concentration in concentrated battery electrolytes are caused by strong association of the counterions at higher concentrations (see Fig. 22).

We have developed equations to predict the heat of relaxation (heat of mixing) of battery electrolytes, finding that it is generally negligible compared to resistive, overpotential, and entropic heat generation. We developed a method to measure entropy by determining the temperature dependence of the potentia,l and we applied it to measure the entropy in six major active materials in Li batteries.

We examined the properties of the SEI layer on Li-Sn negative electrodes and compared the SEI behavior in ether and carbonate electrolytes. This layer can form between particles in alloy electrodes, leading to poor contact between particles and consequent cell capacity loss.

In on-going work, we have modeled dendrite initiation and propagation and are now focusing our work on modeling the influence of mechanical character of polymers in dendrite initiation, which may be the key in making Li-polymer systems work. We are also developing a model for the growth of the SEI layer and working on models of the tunnel $Li_{0.44}MnO_2$ and $LiFePO_4$ electrodes. Finally we are exploring how electronically conductive polymers might be used for overcharge protection, and how two-polymer laminates might permit an increase in the voltage of Li-polymer cells by using a different polymer adjacent to the positive and negative electrodes.

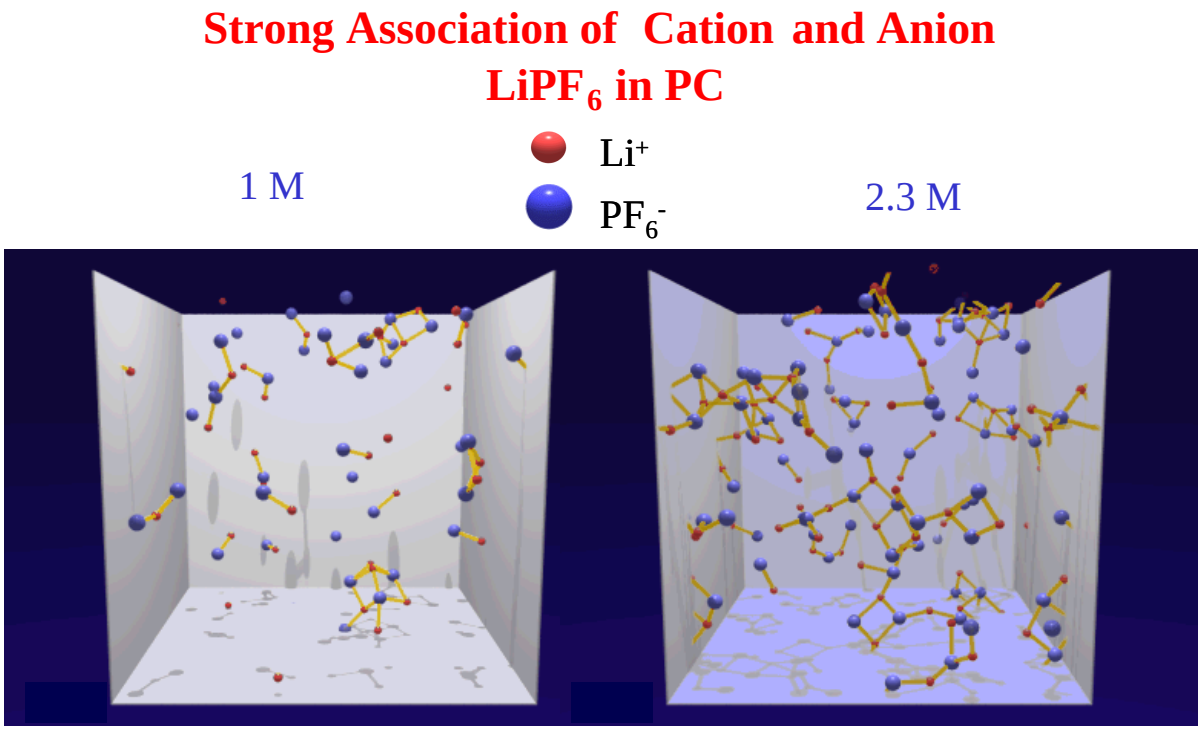

Figure 22. Snapshot of molecular dynamic simulation. Bars indicate strongly associated ion pairs. The presence of more bars at 2.3 M compared to 1 M indicates the reason for increasing viscosity and decreasing conductivity.

Modeling of Electrode Failure Modes (A.M. Sastry, University of Michigan)

Overall, this project has shown the value of first-principles modeling in direct application to design of superior batteries. Our conductivity predictions, based on statistical simulations (Fig. 23), proved extremely accurate when compared with our new experimental results (Fig. 24). These simulations directly accounted for differences in particle shape and amount in the anode, and thus offer a direct means of selecting materials for superior conductivity.

We have now worked on four practical (BATT Program) systems, including low-cost baseline, GDR, SL-25, and Quallion anodes. Our further work will focus on cathodes, with emphasis on understanding the roles of active material conductivity and contact resistance in unwanted ICL.

Our results show conclusively that longer-aspect-ratio particles improve conductivity in anode materials. The amounts of these additives can be modest (~4-5% by volume) to achieve large improvements in conductivity. Contact resistance appears to be affected by particle shape, per our measurements; this is an area meriting further simulation. Battery performance, especially ICL, as it relates to conductivity, is the next major focus area, and a subject of continued collaboration with LBNL (K. Striebel).

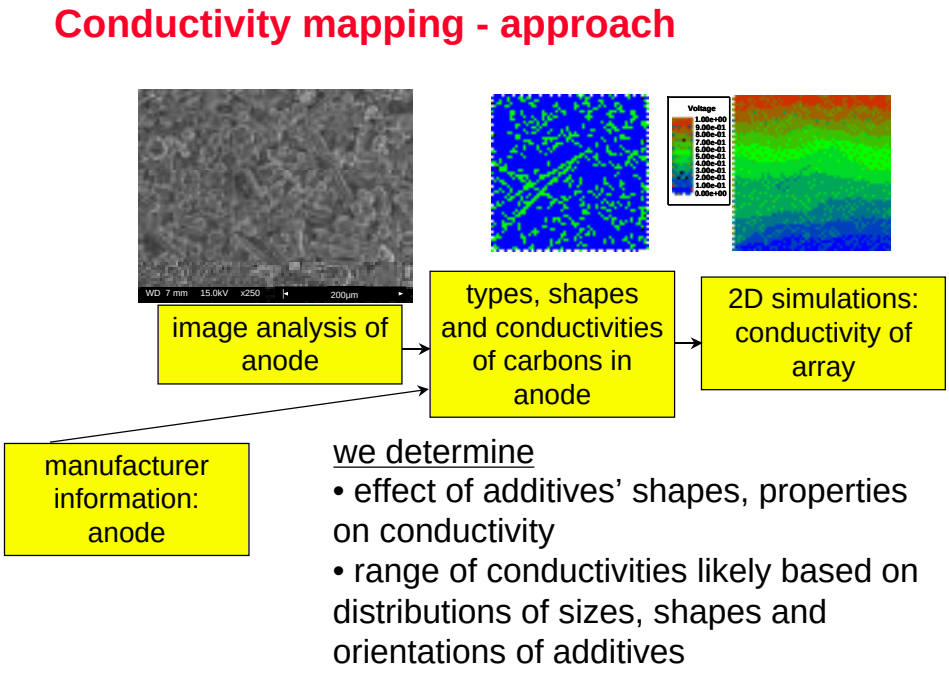

Figure 23. Schematic of approach to image analysis and simulation

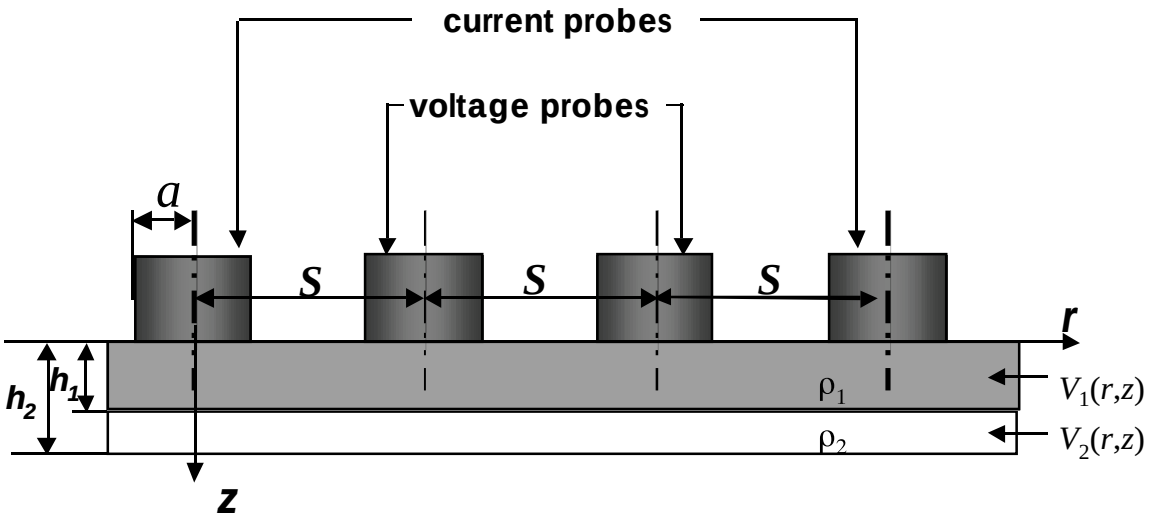

Figure 24. Schematic of four-probe conduction experiment for validation of simulation